International Journal of Biological Macromolecules 337 (2026) 149438

Contents lists available at ScienceDirect

International Journal of Biological Macromolecules

journal homepage: www.elsevier.com/locate/ijbiomac

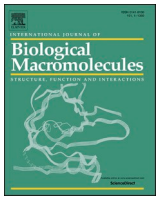

Cactus cladodes as a renewable source of cellulose for the adsorption of Safranin O and Acid Blue 25 dyes: Optimization of extraction parameters, comprehensive experimental investigation, and mechanistic interpretation via Density Functional Theory (DFT)

Soukaina El Bourachdi [a,*], Abdelhay El Amri [b], Ali Raza Ayub [c], Yassine Rakcho [d,e,**], Fatima Moussaoui [a], Fatima Zahra Cherif [e], Mahdi Lechheb [f], Abdelali Grich [g], Javier Araña [h], José Alberto Herrera-Melián [h], Amal Lahkimi [a]

[a] Laboratory of Engineering, Electrochemistry, Modelling and Environment, Faculty of Sciences Dhar El Mehraz, Sidi Mohamed Ben Abdellah University, Fez, Morocco
[b] Laboratory of Advanced Materials and Process Engineering (LAMPE), Faculty of Sciences, Ibn Tofaïl University, B.P. 133, 14000, Kenitra, Morocco
[c] Key Laboratory of Clusters Science of Ministry of Education, School of Chemistry and Chemical Engineering, Beijing Institute of Technology, Beijing, 100081, PR China
[d] Laboratory Materials, Processes, Environment and Quality, National School of Applied Sciences, Cadi Ayyad University (UCA), Route Sidi Bouzid BP 63, 46000, Safi, Morocco
[e] Materials Science, Energy and Nanoengineering (MSN) Department, Mohammed VI Polytechnic University, Lot 660 – Hay Moulay Rachid, 43150, Ben Guerir, Morocco
[f] Materials Sciences for Energy and Sustainable Development Team, Department of Chemistry, FST Errachidia, Moulay Ismail University, Errachidia, Morocco
[g] Laboratory of Analytical and Molecular Chemistry, Faculty Poly-disciplinary of Safi, BP 4162, Safi, 46 000, Morocco
[h] Departamento de Química, Universidad de Las Palmas de Gran Canaria, Edificio de Ciencias Basicas, Campus de Tafira, 35017, Las Palmas de Gran Canaria, Spain

ARTICLE INFO

Keywords:
Acid Blue 25
Adsorption
Cactus cladodes
Cellulose extraction
Density Functional Theory (DFT)
Design-Expert
Safranin O

ABSTRACT

This study focuses on the extraction of cellulose from cactus cladodes in Las Palmas, Canary Islands, and its application for removing Safranin O and Acid Blue 25 dyes. The cellulose extraction process was optimized using Design-Expert software to maximize the BET surface area. The optimal conditions identified were 15 % NaOH, 98 °C, and 90 min, which resulted in a maximum surface area of 7.7890 m^2/g. The adsorption of Safranin O and Acid Blue 25 was evaluated under varying conditions such as contact time, adsorbent mass, pH, initial dye concentration, and temperature. Safranin O exhibited a higher removal efficiency (91.98 %) compared to Acid Blue 25 (41.12 %). The adsorption kinetics followed the Pseudo-Second-Order model, indicating that chemisorption was the rate-limiting step. The Langmuir isotherm best described the adsorption behavior for both dyes, suggesting monolayer adsorption. Safranin O showed a significantly higher maximum adsorption capacity (124.38 mg/g) compared to Acid Blue 25 (11.07 mg/g). Thermodynamic studies revealed that Safranin O adsorption was exothermic and spontaneous, while Acid Blue 25 adsorption was non-spontaneous. Density Functional Theory (DFT) calculations provided further insights into the adsorption mechanism. This study demonstrates the potential of cactus-derived cellulose as an efficient and sustainable adsorbent for dye removal. The integration of experimental data and computational insights offers a comprehensive understanding of the adsorption mechanisms, which can guide the optimization of cellulose-based materials for wastewater treatment applications.

1. Introduction

The excessive use of synthetic dyes in industries such as textiles, paper, plastics, and cosmetics has led to serious environmental and health concerns [1]. Industrial effluents containing these dyes are often discharged without adequate treatment, resulting in the accumulation of toxic and persistent pollutants in aquatic systems [2]. Among them, Safranin O and Acid Blue 25 are of particular concern due to their high

* Corresponding author.
** Correspondence to: Y. Rakcho, Laboratory Materials, Processes, Environment and Quality, National School of Applied Sciences, Cadi Ayyad University (UCA), Route Sidi Bouzid BP 63, 46000, Safi, Morocco.
E-mail addresses: Soukaina.Elbourachdi@usmba.ac.ma (S. El Bourachdi), yassine.rakcho@ced.uca.ma (Y. Rakcho).

https://doi.org/10.1016/j.ijbiomac.2025.149438
Received 22 September 2025; Received in revised form 20 November 2025; Accepted 1 December 2025
Available online 3 December 2025

stability and resistance to biodegradation [3]. Safranin O, a cationic dye widely used in textiles and biological staining, causes intense water discoloration and limits light penetration in aquatic environments, disrupting photosynthesis and threatening aquatic life [4].

Beyond its ecological effects, Safranin O poses serious risks to human health [5]. It can cause skin irritation, allergic reactions, and respiratory discomfort upon contact [6]. Moreover, its mutagenic and carcinogenic properties have been reported, with long-term exposure potentially leading to DNA damage and chronic diseases, emphasizing its hazardous nature.

Similarly, Acid Blue 25, an anionic dye widely used in textiles and leather industries, poses serious environmental and health risks [7]. Its high water solubility allows it to spread easily in aquatic systems, forming toxic byproducts and resisting biodegradation [8]. This persistence leads to bioaccumulation and toxicity in aquatic organisms, disrupting metabolism and reproduction. For humans, exposure to Acid Blue 25 can cause skin irritation, allergic reactions, and, in severe cases, respiratory or liver toxicity [9].

Safranin O and Acid Blue 25 illustrate the persistence of synthetic dye pollution in the environment. Their resistance to biodegradation necessitates advanced and sustainable treatment methods. Developing eco-friendly adsorbents and oxidation processes is therefore essential to protect aquatic ecosystems, human health, and water resources [9].

To address the environmental and health issues associated with dye pollution, various dye removal techniques have been developed over the years. These include physical, chemical, and biological methods such as coagulation- flocculation [10], membrane filtration [11], advanced oxidation processes (AOPs) [12]. Although these methods can be effective in reducing dye concentrations in wastewater, they come with significant drawbacks. For instance, chemical methods often involve the use of harmful reagents that generate secondary pollutants, while physical methods like membrane filtration and coagulation can be expensive and require frequent maintenance.

Among the various wastewater treatment methods including coagulation–flocculation, oxidation, electrochemical degradation, membrane filtration, and biological processes adsorption has emerged as a preferred and highly efficient approach for dye removal [8]. Adsorption offers several distinct advantages over traditional techniques [13]. It is cost-effective, as it often employs low-cost adsorbents such as activated carbon, biochar, or agricultural by-products, making it suitable for large-scale applications [14]. The process is simple and easy to operate, requiring minimal technical expertise and maintenance, which facilitates implementation even in regions with limited resources [15]. Adsorption is known for its high efficiency in removing a wide range of contaminants, including dyes, even at low concentrations. Furthermore, it offers selectivity, as adsorbent surfaces can be chemically modified to target specific pollutants, enhancing treatment performance [16]. A significant merit of adsorption is its regenerability, since many adsorbents can be reused multiple times, reducing operational costs and waste generation. Additionally, adsorption produces minimal toxic byproducts, unlike many chemical or oxidative methods, which often generate hazardous residues. These combined advantages cost-effectiveness, simplicity, efficiency, selectivity, regenerability, and environmental safety position adsorption as one of the most sustainable and promising alternatives for the treatment of dye-contaminated wastewater, providing both environmental and economic benefits [17].

Recent research has focused on the use of natural and renewable materials as adsorbents to make the adsorption process more sustainable and economically viable [18]. Natural materials such as clay, activated carbon, and biomass-derived adsorbents have been widely studied for their potential in dye removal. Among these, cellulose has gained particular attention due to its abundance, renewability, and excellent adsorption properties [19]. Cellulose is a biopolymer composed of glucose units, which provide a high surface area and numerous hydroxyl functional groups that interact with dye molecules [20].

Cactus plants, abundant in arid and semi-arid regions, present a promising and sustainable source of cellulose for adsorption applications, contributing to environmental preservation and resource efficiency [21]. Renowned for their ability to thrive in extreme conditions with minimal water and maintenance, cacti are well-suited for regions where water scarcity poses challenges [22]. In areas like Las Palmas, situated in the Canary Islands, cactus cultivation has long-standing historical and cultural significance [23]. The region's unique climate fosters the growth of various cactus species, and these plants have been integral to local practices, serving as a source of food, livestock feed, and natural barriers against wind and soil erosion. Over time, researchers have begun exploring the broader environmental applications of cactus, uncovering its potential for water purification and pollutant removal, particularly in adsorption processes [24].

The extraction of cellulose from cactus represents a renewable and biodegradable solution for tackling pollution, particularly the removal of harmful dyes from wastewater [25]. This approach promotes the sustainable utilization of local natural resources while aligning with global initiatives to minimize industrial waste and reduce reliance on non-renewable materials [26]. The use of cactus-derived cellulose also encourages circular economic practices, converting an abundant and underutilized plant into a high-value material for environmental remediation [27]. By integrating these sustainable solutions into traditional practices in regions like Las Palmas, communities can achieve both economic and ecological benefits.

Cactus-derived cellulose is uniquely suited for adsorption applications due to its exceptional structural and chemical properties [28]. The material boasts a highly porous structure and a rich array of functional groups, including hydroxyl and carboxyl groups, which facilitate strong interactions with pollutants [29]. These attributes enable it to adsorb both cationic and anionic dyes effectively, making it ideal for the simultaneous removal of pollutants such as Safranin O and Acid Blue 25. This dual capability addresses a significant challenge in wastewater treatment, as many adsorbents are selective for specific dye types [30]. Moreover, the reliance on cactus-derived cellulose reduces dependency on synthetic adsorbents, which are often expensive, energy-intensive to produce, and environmentally detrimental [31].

The integration of cactus-derived cellulose in dye adsorption processes offers numerous advantages, particularly in regions like Las Palmas, where cactus is readily available. This approach supports the development of sustainable and cost-effective wastewater treatment systems that utilize local materials. By leveraging the natural properties of cactus, it is possible to create adsorbents that are not only efficient but also biodegradable and easy to regenerate. Furthermore, the use of cactus-derived cellulose aligns with the circular economy model, promoting resource efficiency and waste reduction. Las Palmas provides an ideal setting for this type of research due to its rich biodiversity and long-standing traditions of utilizing cactus in various industries. The cultivation of cactus in this region not only sustains local economies but also offers an environmentally friendly resource for addressing global water pollution challenges.

The primary objective of this study is to evaluate the potential of cellulose extracted from cactus plants as an efficient, sustainable, and environmentally friendly adsorbent for the removal of Safranin O and Acid Blue 25 dyes from aqueous solutions. This investigation arises from the growing need for low-cost and renewable materials capable of addressing the persistent problem of dye contamination in industrial wastewater.

The research begins with the extraction of cellulose through an alkaline treatment process, focusing on the optimization of critical parameters such as sodium hydroxide (NaOH) concentration, treatment temperature, and treatment time, which significantly influence the BET surface area (m^2/g) and the overall quality of the extracted cellulose. To ensure the optimization of these parameters, a systematic experimental design was adopted, allowing for the identification of the best operating conditions that yield cellulose with enhanced adsorption properties.

Following the extraction, the structural, morphological, and surface

characteristics of the resulting cellulose were thoroughly examined using multiple analytical techniques. The pH at the point of zero charge (pHpzc) was determined to evaluate the surface charge behavior and its influence on dye adsorption. Fourier Transform Infrared Spectroscopy (FTIR) was employed to identify the functional groups responsible for the adsorption interactions, while X-ray Diffraction (XRD) analysis provided insights into the crystalline structure and degree of crystallinity of the cellulose. In addition, Scanning Electron Microscopy (SEM) was used to visualize the surface morphology, texture, and porosity of the adsorbent.

The adsorption capacity of the prepared cellulose was then investigated for the simultaneous removal of Safranin O and Acid Blue 25 dyes, chosen as representative cationic and anionic pollutants, respectively. The effects of various operational parameters including initial dye concentration, contact time, pH, temperature, and adsorbent dosage were systematically examined and optimized to achieve maximum adsorption efficiency. To gain a deeper understanding of the adsorption mechanism, the equilibrium data were analyzed using different isotherm models (Langmuir, Freundlich, and Temkin) to describe the surface homogeneity, adsorption capacity, and nature of interactions between the dyes and the adsorbent. Furthermore, kinetic models such as the pseudo-first-order and pseudo-second-order were applied to interpret the adsorption rate and identify the controlling mechanisms governing the process.

Beyond the experimental work, a theoretical study was conducted to provide molecular-level insights into the adsorption mechanism and to complement the experimental findings. This computational investigation aimed to elucidate the possible electrostatic and hydrogen-bonding interactions occurring between the dye molecules and the active sites on the cellulose surface. By integrating experimental and theoretical analyses, this study offers a comprehensive understanding of the structure–property–performance relationship, thereby highlighting the scientific and environmental significance of cactus-derived cellulose as a promising bioadsorbent for sustainable wastewater treatment.

Despite these valuable findings, the present study has certain limitations that should be acknowledged. All adsorption experiments were conducted under controlled laboratory conditions using synthetic dye solutions, which, while suitable for mechanistic understanding, do not fully represent the complex composition of real industrial wastewater. Actual effluents typically contain a diverse mixture of pollutants including salts, surfactants, heavy metals, and organic compounds that may compete for adsorption sites, potentially reducing the adsorption efficiency. Moreover, parameters such as pH, ionic strength, and temperature in industrial wastewater can fluctuate significantly, further influencing the adsorbent's performance and stability.

Another limitation lies in the absence of large-scale application and regeneration tests. While the study demonstrates the efficiency of cactus-derived cellulose at the laboratory scale, additional research is required to evaluate its reusability, mechanical stability, and long-term adsorption capacity under realistic operating conditions. Furthermore, the environmental impact and cost-effectiveness of cellulose production at a larger scale should also be examined to validate its practical feasibility.

Future research should therefore focus on the application of this bioadsorbent to real industrial effluents, assessment of its reusability and regeneration potential, and exploration of surface modification or composite formation to further enhance adsorption selectivity and capacity. Such studies would contribute to translating the present findings into real-world environmental remediation technologies.

2. Material and methods

2.1. Chemicals and reagents

The chemicals and reagents used in this study include hydrochloric acid (HCl, 37 % w/w), sodium hydroxide (NaOH, ≥98 % purity), hydrogen peroxide (H_2O_2, 30 % w/w), and acetic acid (CH_3COOH, ≥99 % purity), all of analytical grade and purchased from Sigma-Aldrich. The target dyes for adsorption experiments were Safranin O ($C_{20}H_{19}ClN_4$, molecular weight: 350.84 g/mol, ≥98 % purity) and Acid Blue 25 ($C_{20}H_{13}N_2NaO_5S$, molecular weight: 416.38 g/mol, ≥95 % purity) [32]. Safranin O is a cationic dye with a maximum absorption wavelength (λ_{max}) of approximately 520 nm [3], while Acid Blue 25 is an anionic dye exhibiting a λmax of around 600 nm, both of which were detected and quantified using UV–visible spectrophotometry.

2.2. Extraction of cellulose and optimization

Cellulose was extracted from fresh cactus cladodes collected from Las Palmas, Canary Islands. The cladodes were air-dried for 2 days, cut into 1–2 cm pieces, and ground into fine powder. The powdered cactus material underwent an initial treatment with hot water at 70 °C for 2 h to remove soluble impurities and surface contaminants [33]. The resulting material was centrifuged at 4000 rpm to obtain cellulose-rich fibers. To optimize the cellulose extraction process, the cactus fibers were subjected to alkaline treatment with varying NaOH concentrations (10–15 %), at treatment temperatures (60–98 °C), and for treatment times (90–300 min) ensuring the removal of residual hemicellulose, lignin, fats, and waxes [34]. The experimental parameters were designed and evaluated based on their influence on the BET surface area (m^2/g) of the extracted cellulose. After the treatment, the cellulose were thoroughly washed with distilled water to neutralize the pH and then treated with hydrogen peroxide (H_2O_2) for decoloration [35]. The cellulose content of the raw cactus biomass was evaluated by applying the Updegraff method for cellulose isolation, followed by quantification using the anthrone colorimetric assay. The plant fibers were treated with a mixture of acetic acid and nitric acid to remove lignin, hemicellulose, and xylans, leaving cellulose as the main component. The cellulose was subsequently hydrolyzed to glucose, and the total sugar content in solution was determined using the anthrone reagent. Anthrone solution was prepared by dissolving 10 mg of anthrone in 100 mL of 70 % sulfuric acid. A calibration curve was constructed by reacting known concentrations of glucose with anthrone reagent and measuring absorbance at 625 nm using a spectrophotometer [36,37]. The cellulose content of the raw cactus material was found to be approximately 18.5 ± 1.2 %, confirming that cactus is a suitable source for cellulose extraction. Finally, the purified cellulose was air-dried under ambient conditions to prepare it for subsequent characterization and adsorption experiments. Fig. 1 shows the extraction process of cellulose.

In this study, the Design-Expert software (version 13.0.5.0) was used to perform a 2-level factorial design for optimizing the extraction conditions of cellulose from cactus. This software is a powerful tool for designing experiments, analyzing results, and building statistical models to understand the relationship between multiple factors and responses [38]. The factorial design employed in this study was randomized to eliminate any potential bias from uncontrolled variables that might affect the results [39].

The 3FI model used in this study represents a 3-factor interaction model, allowing us to evaluate the main effects of each factor as well as the interactions between factors. The three factors under consideration were: NaOH concentration, treatment temperature, and treatment time. The Design-Expert software enables the efficient optimization of these parameters [40], as it can predict the effects of these factors on the BET surface area of the extracted cellulose, which is critical for understanding its adsorption capacity. Table 1 shows the Experimental Design Parameters for Cellulose Extraction Optimization.

In the factorial design, each factor was varied at two levels, resulting in a total of 8 experimental runs. The factors were NaOH concentration (10–15 %), treatment temperature (60 °C–98 °C), and treatment time (90–300 min). The randomization of these runs ensures that the outcomes are not influenced by any external factors such as the sequence of experimental steps. The software provides statistical analysis of the

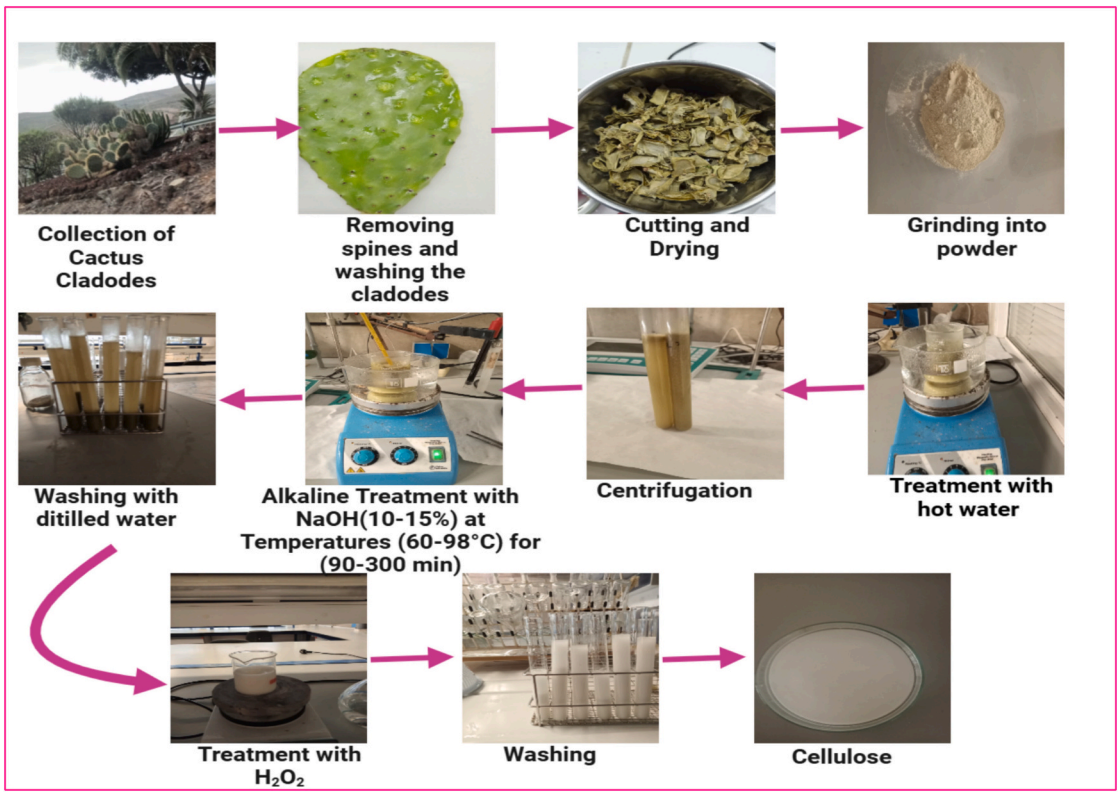

Fig. 1. Extraction process of cellulose from cactus cladodes.

Table 1
Experimental design parameters for cellulose extraction optimization.

Factor	Name	Units	Type	Minimum	Maximum	Mean
A	Concentration of NaOH	%	Numeric	10.00	15.00	12.50
B	Treatment temperature	°C	Numeric	60.00	98.00	79.00
C	Treatment time	Min	Numeric	90.00	300.00	195.00

interaction effects between the factors, which helps in identifying the optimal extraction conditions for obtaining the best cellulose material for dye adsorption.

One of the key benefits of using Design-Expert is its ability to model and predict the effects of multiple variables simultaneously [26]. In this study, it helped in understanding how each factor influences the surface area of the extracted cellulose, thereby affecting its performance as an adsorbent for the removal of Safranin O and Acid Blue 25 dyes.

2.3. Characterization

The cactus-derived cellulose was characterized using a comprehensive set of analytical techniques to evaluate its structural, surface, and morphological properties both before and after adsorption of Safranin O and Acid Blue 25. Fourier-transform infrared spectroscopy (FTIR, Bruker Tensor 27) was conducted in the range of 4000–400 cm^{-1} using the KBr pellet method, where approximately 1 mg of cellulose was finely ground with 100 mg of KBr and pressed into a pellet. This analysis was used to identify functional groups and monitor chemical bond changes resulting from dye adsorption [8]. X-ray diffraction (XRD, PANalytical X'Pert PRO) with Cu Kα radiation (λ = 1.5406 Å) operated at 40 kV and 40 mA was employed to determine the crystalline structure and degree of crystallinity, scanning 2θ angles from 5° to 80° with a step size of 0.02° and a scanning speed of 1°/min. Brunauer–Emmett–Teller (BET) surface area analysis was performed using a Micromeritics ASAP 2020 analyzer, with nitrogen adsorption–desorption isotherms measured at 77 K. Samples were degassed at 120 °C for 12 h under vacuum prior to measurement to remove moisture and contaminants. BET analysis provided the specific surface area, total pore volume, and average pore diameter, while the Barrett–Joyner–Halenda (BJH) method was applied to analyze pore size distribution [41]. The surface morphology and porosity were examined using scanning electron microscopy (SEM, JEOL JSM-6510) at an accelerating voltage of 10–15 kV. Samples were coated with a thin gold layer (~5 nm) under vacuum to ensure electrical conductivity and prevent charging. SEM imaging allowed visualization of the cellulose's surface texture, pore structure, and any structural changes induced by dye adsorption.

2.3.1. Surface charge and point of zero charge (pHpzc)

The surface charge of the cactus-derived cellulose was evaluated by determining its point of zero charge (pHpzc), which is a crucial parameter for understanding the electrostatic interactions between the adsorbent and the adsorbates. The pHpzc is the pH at which the net surface charge of the material is zero, meaning that there is no overall electrostatic attraction or repulsion between the adsorbent surface and the surrounding solution. To determine the pHpzc of the cellulose, a batch adsorption experiment was performed where a fixed amount of cellulose was added to aqueous solutions with varying pH levels [42]. The pH of the solution was adjusted using acid (HCl) or base (NaOH), and the final pH was measured after equilibrating the system [43]. The pHpzc was determined by plotting the pH of the solution versus the number of adsorbed ions. At the pH where there is no change in the pH

of the solution, the surface charge of the cellulose is considered neutral [44].

3. Adsorption

3.1. Adsorbate preparation

The preparation of the adsorbates, Safranin O and Acid Blue 25, involved the preparation of stock solutions at a concentration of 1 g/L. For this, 1 g of each dye was precisely weighed using an analytical balance and dissolved in 1 L of distilled water. The solutions were mixed thoroughly by stirring to ensure complete dissolution of the dyes, resulting in homogeneous solutions. This 1 g/L concentration was chosen for the experiments to evaluate the adsorption capacity of cactus-derived cellulose and to study the interaction of the material with the dyes. The prepared solutions were stored in clean, properly labeled containers for future use in adsorption experiments, which were designed to assess various parameters, including adsorption kinetics, equilibrium, and the optimization of the adsorption process for efficient dye removal.

3.2. Study of adsorption kinetics

3.2.1. Effect of contact time

To investigate the adsorption kinetics of Safranin O and Acid Blue 25 on cactus-derived cellulose, the effect of contact time on the adsorption process was analyzed. In each experiment, 0.1 g of cellulose was added to 50 mg/L dye solutions (either Safranin O or Acid Blue 25) and stirred for periods ranging from 10 min to 220 min. Samples were taken at various time intervals (10, 30, 60, 90, 120, 150, 180, 210, and 220 min) to monitor the progress of dye removal. Dye concentrations in the solution were measured using a spectrophotometer at 518 nm for Safranin O and 617 nm for Acid Blue 25. The adsorption capacity at equilibrium, Qe (mg/g), was calculated using Eq. (1) [45]:

$$\boldsymbol{Q_e} = (\boldsymbol{C_i} - \boldsymbol{C_e}) \times \frac{\boldsymbol{V}}{\boldsymbol{m}} \tag{1}$$

The percentage of dye removal (R%) was determined using the Eq. (2):

$$\boldsymbol{R}\% = \left(\frac{\boldsymbol{C_i} - \boldsymbol{C_e}}{\boldsymbol{C_i}}\right) \times \mathbf{100} \tag{2}$$

where: C_o and C_e are the initial and equilibrium dye concentrations (mg/L), V is the solution volume (L), and m is the mass of the adsorbent (g).

3.3. Study of dye adsorption kinetics

3.3.1. Modeling the adsorption kinetics

To further understand the adsorption process of Safranin O and Acid Blue 25 onto cactus-derived cellulose, the adsorption kinetics were modeled using two common models: the pseudo-first-order and pseudo-second-order models [46]. These models describe the rate of dye uptake by the adsorbent and help determine the nature of the adsorption process.

The pseudo-first-order model (also known as the Lagergren model) assumes that the rate of adsorption is proportional to the difference between the equilibrium dye concentration and the dye concentration at time t [47]. The linear form of the pseudo-first-order equation is expressed by Eq. (3):

$$\boldsymbol{ln}(\boldsymbol{Q_e} - \boldsymbol{Q_t}) = \boldsymbol{lnQ_e} - \boldsymbol{k_1 t} \tag{3}$$

where Q_e (mg/g) is the adsorption capacity at equilibrium, Q_t (mg/g) is the adsorption capacity at time t, k_1 (min^{-1}) is the first-order rate constant, and t (min) is the contact time.

The pseudo-second-order model assumes that the rate of adsorption is proportional to the square of the difference between the equilibrium concentration and the dye concentration at time t [48]. The linear form of the pseudo-second-order equation is expressed by Eq. (4):

$$\frac{\boldsymbol{t}}{\boldsymbol{Q_t}} = \frac{\mathbf{1}}{\boldsymbol{k_2}(\boldsymbol{Q_e})^2} + \frac{\boldsymbol{t}}{\boldsymbol{Q_e}} \tag{4}$$

where: k_2 (g/mg·min) is the second-order rate constant. Both models were applied to the experimental data to evaluate their fitting. The adsorption capacity (Q_e) and rate constant (k_1 and k_2) were determined from the slopes and intercepts of the corresponding plots. The correlation coefficients (R^2) of both models were compared to identify the most suitable model for describing the adsorption kinetics of Safranin O and Acid Blue 25 onto cactus-derived cellulose [49].

3.4. Identification of optimum adsorption conditions

The optimum adsorption conditions for Safranin O and Acid Blue 25 removal using cactus-derived cellulose were determined by evaluating the effects of adsorbent mass, pH, dye concentration, and temperature. The adsorbent mass varied from 0.03 to 0.19 g, while the pH was adjusted between 2 and 10. Dye concentrations in the range of 50 to 250 mg/L were tested, and the temperature was varied from 25 °C to 55 °C. These parameters were systematically optimized to identify the most effective conditions for the adsorption process.

3.4.1. The Langmuir model

The adsorption isotherms of Safranin O and Acid Blue 25 onto cactus-derived cellulose were analyzed using the Langmuir model, which assumes monolayer adsorption onto a surface with a finite number of identical adsorption sites [50]. According to this model, the adsorption capacity increases as the dye concentration in the solution rises until the surface reaches saturation.

The Langmuir model is characterized by a maximum adsorption capacity (Q_m) and a Langmuir constant (K_L), which are determined from the linear form of the isotherm. The Langmuir equation is expressed by Eq. (5):

$$\frac{C_e}{Q_e} = \frac{1}{K_L Q_m} + \frac{C_e}{Q_m} \tag{5}$$

where: Qe is the amount of dye adsorbed at equilibrium (mg/g), Ce is the equilibrium dye concentration (mg/L), Q_m is the maximum adsorption capacity (mg/g), and K_L is the Langmuir constant.

3.4.2. The Freundlich model

The adsorption of Safranin O and Acid Blue 25 onto cactus-derived cellulose was also examined using the Freundlich isotherm model. Unlike the Langmuir model, which assumes monolayer adsorption, the Freundlich model is based on multilayer adsorption onto heterogeneous surfaces. It assumes that the adsorption sites have a non-uniform distribution of energies, with a higher affinity for adsorption at low concentrations of dye [51]. The Freundlich equation is expressed by Eq. (6):

$$ln(Q_e) = ln(K_F) + \frac{1}{n_F} ln(C_e) \tag{6}$$

where Qe is the amount of dye adsorbed at equilibrium (mg/g), C_e is the equilibrium dye concentration (mg/L), K_F is the Freundlich constant, and $1/n_F$ is the adsorption intensity. The Freundlich model is typically used to describe adsorption on surfaces with varying adsorption energies. A high value of K_F and a low value of $1/n_F$ indicate a favorable adsorption process.

3.4.3. The Temkin model

The Temkin isotherm model was also applied to evaluate the adsorption of Safranin O and Acid Blue 25 onto cactus-derived cellulose.

This model assumes that the heat of adsorption of all molecules in the layer decreases linearly with coverage and that there are no interactions between adsorbed molecules [52]. The Temkin model accounts for adsorbate-adsorbent interactions by incorporating a factor that represents the adsorption potential, which decreases with increasing coverage [45]. The Temkin equation is given by the Eq. (7):

$$ln(Q_e) = \frac{RT}{b} lnK_T + \frac{RT}{b} C_e \quad (7)$$

where: Q_e is the amount of dye adsorbed at equilibrium (mg/g), C_e is the equilibrium dye concentration (mg/L), and b is a constant related to the heat of adsorption (J/mol). The Temkin model is often used to describe adsorption systems where adsorbate-adsorbent interactions play a significant role, and it helps assess the energy distribution of adsorption sites.

3.4.4. Thermodynamic study

The thermodynamic study of the adsorption process of Safranin O and Acid Blue 25 onto cactus-derived cellulose provides valuable insights into the spontaneity, feasibility, and nature of the adsorption process. Several thermodynamic parameters, such as the change in Gibbs free energy (ΔG°), enthalpy (ΔH°), and entropy (ΔS°), were calculated to understand the energetics and driving forces of the adsorption. These parameters were determined using Eqs. (8), (9), and (10) [53]:

$$Ke = \frac{Qe}{Ce} \quad (8)$$

$$lnKe = \frac{\Delta S^\circ}{R} - \frac{\Delta H^\circ}{RT} \quad (9)$$

$$\Delta G^\circ = \Delta H^\circ - T\Delta S^\circ \quad (10)$$

where: R is the universal gas constant (8.314 J/mol·K), T is the temperature (K), and Ke is the equilibrium constant derived from the adsorption isotherm. A negative ΔG° value indicates a spontaneous adsorption process, while a positive ΔG° suggests non-spontaneity. The enthalpy change (ΔH°) provides information on the nature of the adsorption, with a negative value indicating an exothermic process and a positive value indicating an endothermic process. The entropy change (ΔS°) reflects the degree of disorder or randomness associated with the adsorption process, with a positive value suggesting an increase in disorder.

4. Density Functional Theory study

In this study, Density Functional Theory (DFT) calculations were employed to comprehensively analyze the interaction between cellulose extracted from cactus and the dyes Safranin O and Acid Blue 25 [54]. The primary aim was to uncover the molecular-level adsorption mechanisms and to explore how the electronic properties of cellulose influence its adsorption capacity for these dyes. Using the B3LYP hybrid functional method combined with the 6-31G(d,p) basis set, the molecular geometries of cellulose and the dyes were optimized, and critical electronic properties, including the energies of the Highest Occupied Molecular Orbital (HOMO) and the Lowest Unoccupied Molecular Orbital (LUMO), were computed [55]. These properties provided essential insights into the stability and reactivity of the dye-cellulose complexes. The HOMO and LUMO energies were utilized to evaluate the potential for electron transfer between the dye molecules and the cellulose surface, a key factor influencing adsorption efficiency [56]. The calculated energy gap (ΔEgap) between the HOMO and LUMO serves as an important indicator of adsorption strength, with a smaller gap suggesting enhanced interaction and efficient electron transfer [57]. The optimized molecular structures revealed that the hydroxyl groups (-OH) on the cellulose surface play a pivotal role in adsorption through hydrogen bonding, complemented by potential electrostatic interactions with the charged dye molecules. In addition to the energy gap, other electronic properties were calculated, including the electronic chemical potential (μ), hardness (η), softness (S), and electrophilicity (ω) using Eqs. (11), (12), (13), (14), and (15):

$$\Delta E_{Gap} = E_{Lumo} - E_{Homo} \quad (11)$$

$$\eta = \frac{E_{Lumo} - E_{Homo}}{2} \quad (12)$$

$$x = \frac{-(E_{Homo} - E_{Lumo})}{2} \quad (13)$$

$$S = \frac{1}{\eta} \quad (14)$$

$$\omega = \frac{x^2}{2\eta} \quad (15)$$

These parameters offer deeper insights into the material's reactivity. The chemical potential reflects the system's electron affinity, while hardness and softness indicate resistance to electron deformation and overall molecular reactivity [58]. Electrophilicity measures the system's propensity to accept electrons. DFT calculations also highlighted electronic density shifts in cellulose upon interaction with the dyes, reinforcing the role of specific molecular interactions in enhancing the adsorption process. These findings provide valuable insights into the structural and electronic factors underlying the adsorption mechanisms.

5. Optimization results

5.1. Influence of treatment parameters on BET surface area

In order to evaluate the effect of NaOH concentration, treatment temperature, and treatment time on the surface properties of cellulose, a series of experiments were conducted to determine the BET surface area. These factors are crucial for enhancing the surface area and, consequently, the adsorption capacity of cellulose-based materials. The experimental results demonstrate how variations in these conditions influence the surface area of cellulose, providing insights into the optimal conditions for enhancing adsorption performance.

The experimental results in Table 2 demonstrate the influence of NaOH concentration, treatment temperature, and treatment time on the BET surface area of cellulose. The surface area values ranged from 2.5643 m^2/g to 7.7890 m^2/g, depending on the varying conditions. The highest surface area, 7.7890 m^2/g, was achieved under a 15 % NaOH concentration, a treatment temperature of 98 °C, and a treatment time of 90 min. This result indicates that higher NaOH concentrations and elevated temperatures significantly enhance the surface area of the cellulose, likely due to the increased alkali-induced swelling and the removal of impurities, which open up the cellulose structure [59].

Conversely, the lowest surface area of 2.5643 m^2/g was observed

Table 2
BET surface area results for cellulose extraction under various treatment conditions.

	Concentration of NaOH (%)	Treatment temperature (°C)	Treatment time (min)	BET surface area (m^2/g)
1	15	60	90	6.5673
2	10	60	300	2.5643
3	15	98	90	7.7890
4	10	98	300	4.3911
5	10	60	90	3.1578
6	15	60	300	6.1128
7	10	98	90	5.2091
8	15	98	300	6.9923

with a 10 % NaOH concentration, a treatment temperature of 60 °C, and a longer treatment time of 300 min. This suggests that lower NaOH concentrations and milder temperatures may not sufficiently disrupt the cellulose structure, leading to a less effective treatment [60]. Additionally, prolonged treatment times at lower temperatures may not offer significant benefits, as the effects of NaOH concentration and temperature are more critical in enhancing the surface area.

5.2. BET isotherm behavior of cellulose extracted under different treatment conditions

To further investigate the structural properties of the treated cellulose, BET isotherms were obtained, revealing key insights into the mesoporous nature of the material [61]. Fig. 2 shows that the isotherms exhibited Type IV behavior, which is characteristic of mesoporous materials with pore sizes ranging from 2 to 50 nm [62]. This behavior included a linear region at lower relative pressures (P/P_o), corresponding to monolayer and multilayer adsorption on the walls of mesopores, followed by a gradual increase at intermediate pressures. Although the presence of a hysteresis loop, typically indicative of capillary condensation in mesoporous, was not explicitly mentioned, the overall behavior strongly suggests mesoporosity. At higher relative pressures, the isotherms plateaued, signifying the saturation of adsorption sites and the filling of mesopores. The mesoporous structure of the treated cellulose was significantly influenced by the NaOH concentration, temperature, and treatment duration. Higher NaOH concentrations (15 %) and elevated temperatures (98 °C) promoted the development of mesoporous, resulting in larger surface areas. The highest BET surface area, 7.7890 m^2/g, was achieved under optimal conditions (15 % NaOH, 98 °C, 90 min). In contrast, lower NaOH concentrations (10 %) or prolonged treatment durations (300 min) resulted in less pronounced mesoporosity, likely due to cellulose degradation or pore collapse.

5.3. Statistical analysis of factors influencing BET surface area: half-normal plot and Pareto Chart evaluation

The significance of three factors NaOH concentration (A), treatment temperature (B), and treatment time (C) on the BET surface area was evaluated using a Half-Normal Plot (Fig. 3a) and a Pareto Chart (Fig. 3b), along with the interaction effects of AC and BC. The Half-

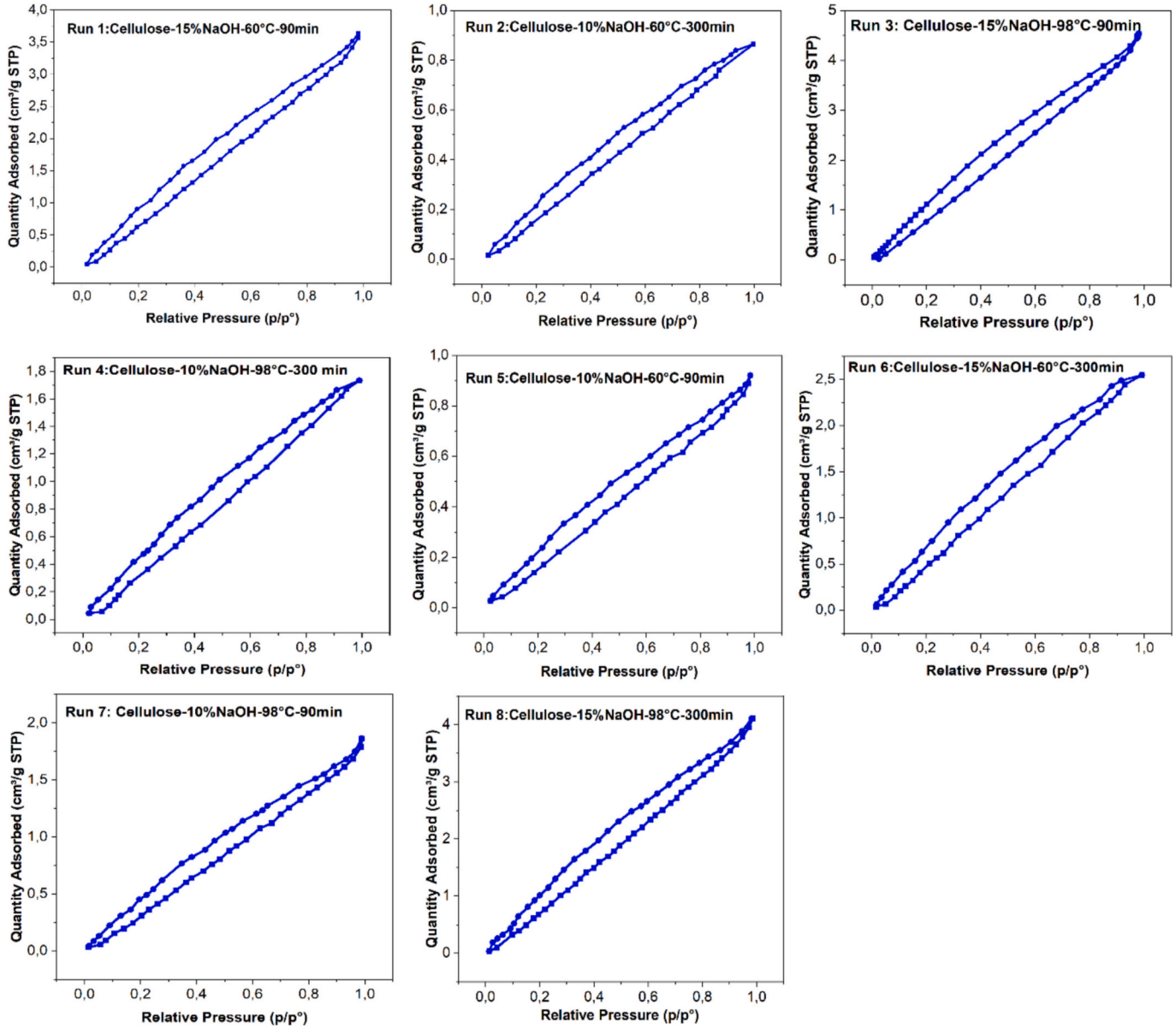

Fig. 2. BET adsorption isotherms of cellulose under various alkaline treatment conditions.

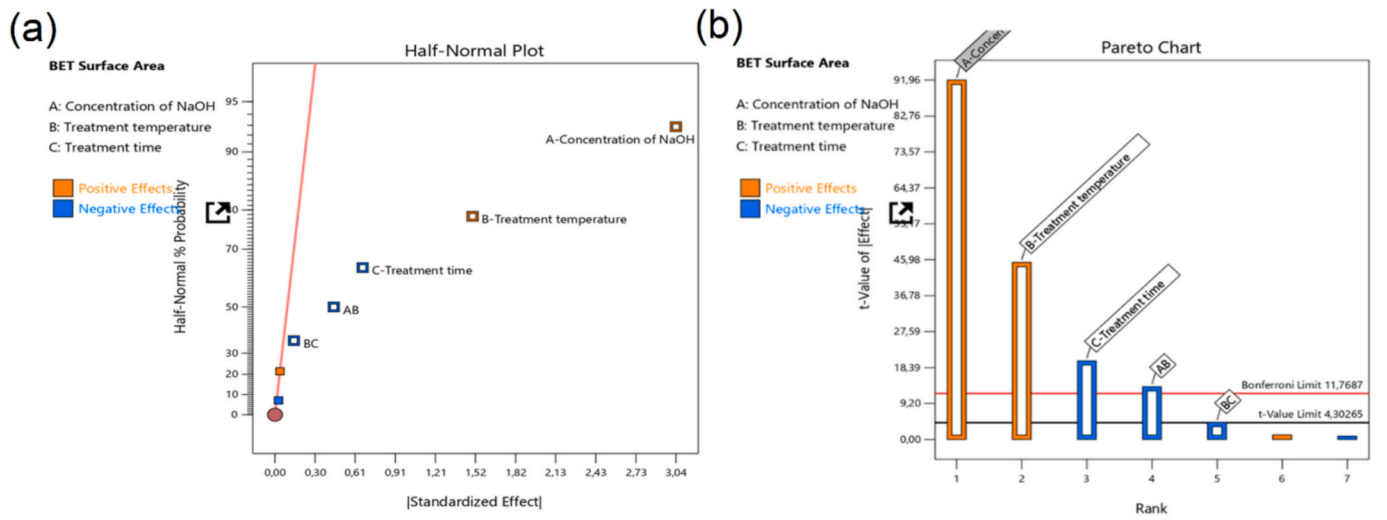

Fig. 3. Half-normal and Pareto Charts for BET surface area analysis.

Normal Plot visually indicates which factors significantly affect the BET surface area by showing the points furthest from the normal probability line. Factor A, the concentration of NaOH, demonstrates the greatest deviation, followed by factor B, treatment temperature, and the interaction term AC, all of which indicate a substantial positive impact on the BET surface area. Conversely, factor C, treatment time, and the interaction term BC lie closer to the line, suggesting their influence is less significant. The Pareto Chart further clarifies the significance of these factors by displaying their t-values in descending order [63]. Factors A and B exhibit the highest t-values, significantly exceeding the Bonferroni limit, confirming their critical role in determining the BET surface area. The interaction term AC also exceeds the t-value threshold, underscoring its importance in the model. On the other hand, factor C and the interaction term BC fall below the threshold, indicating their negligible impact. Overall, the results show that NaOH concentration, treatment temperature, and the interaction between NaOH concentration and treatment time (AC) are the key factors in optimizing the BET surface area, whereas treatment time and other interactions have minimal influence.

5.4. Analysis of Variance (ANOVA) for factors influencing BET surface area

The Table 3 presents the Analysis of Variance (ANOVA) results for the model assessing the effects of three factors NaOH concentration (A), treatment temperature (B), and treatment time (C) on the BET surface area. The model is statistically significant, as evidenced by its F-value of 2223.09 and a *p*-value of 0.0004, which is well below the conventional significance threshold (0.05) [64], indicating that the model explains a substantial portion of the variability in the BET surface area. Among the individual factors, A (NaOH concentration) shows the highest sum of squares (18.44), the largest F-value (8456.02), and the smallest *p*-value (0.0001), confirming it as the most significant contributor to the model [65]. B (treatment temperature) also exhibits a notable effect, with a sum of squares of 4.48, an F-value of 2053.70, and a p-value of 0.0005. Although C (treatment time) has a smaller effect, it remains statistically significant, with a sum of squares of 0.8825, an F-value of 404.59, and a p-value of 0.0025.

The interaction term AB (between NaOH concentration and treatment temperature) also shows a moderate effect, with an F-value of 182.19 and a p-value of 0.0054, indicating statistical significance. The interaction term BC (between treatment temperature and treatment time) has the lowest contribution, with a sum of squares of 0.0413 and an F-value of 18.95, though it is still statistically significant with a p-value of 0.0489. The residual error is minimal (sum of squares = 0.0044, mean square = 0.0022), suggesting a good fit for the model [66].

The statistical analysis of the model demonstrates excellent performance in predicting the response variable, as shown in Table 4. With an R^2 value of 0.9998 and an adjusted R^2 of 0.9994, the model explains almost all of the variability in the data, indicating a near-perfect fit [39]. The standard deviation of 0.0467 and the low coefficient of variation (C.V. = 0.8735 %) highlight minimal error and low relative variability in the data, further reinforcing the model's accuracy. Additionally, the predicted R^2 value of 0.9971 suggests excellent generalizability to new data, ensuring the model's robustness. Finally, the high Adeq Precision value of 128.5074 confirms a strong signal-to-noise ratio, indicating reliable predictions.

Table 4
Summary of regression model statistics.

Std. Dev.	0.0467	R^2	0.9998
Mean	5.35	Adjusted R^2	0.9994
C.V. %	0.8735	Predicted R^2	0.9971
		Adeq precision	128.5074

Table 3
Analysis of Variance (ANOVA) for assessing the BET surface area.

Source	Sum of squares	Df	Mean square	F-value	p-Value	
Model	24.24	5	4.85	2223.09	0.0004	Significant
A-Concentration of NaOH	18.44	1	18.44	8456.02	0.0001	
B-Treatment temperature	4.48	1	4.48	2053.70	0.0005	
C-Treatment time	0.8825	1	0.8825	404.59	0.0025	
AB	0.3974	1	0.3974	182.19	0.0054	
BC	0.0413	1	0.0413	18.95	0.0489	
Residual	0.0044	2	0.0022			
Cor Total	24.25	7				

5.5. Model validation through predicted vs. actual BET surface area values

The Fig. 4 effectively demonstrates the reliability of the model by illustrating a strong correlation between the predicted and actual values. The close alignment of data points along the diagonal line (y = x) suggests that the model is highly accurate, with minimal deviation between predictions and observations. Additionally, the points, which represent BET Surface Area values ranging from approximately 2.56 to 7.79, show no systematic pattern or bias in prediction errors across the range of surface area values.

5.6. Individual effects

The Fig. 5 illustrates the individual effects of NaOH concentration (A), treatment temperature (B), and treatment time (C) on the BET Surface Area (m^2/g), along with warnings about significant factor interactions. In Fig. 5(a), the BET Surface Area increases with higher NaOH concentration, indicating a positive impact, but the warning suggests an interaction between NaOH concentration and temperature. The Fig. 5(b) shows an increase in BET Surface Area with rising treatment temperature, highlighting its importance, though it is involved in multiple interactions. In contrast, The Fig. 5(c) reveals a slight decrease in BET Surface Area with prolonged treatment time, suggesting a negative effect, with a warning pointing to its interaction with temperature. These findings emphasize the need to account for factor interactions when optimizing conditions to maximize BET Surface Area.

5.7. Response surface and contour analysis of BET surface area optimization

The response surface and contour plots provide a detailed analysis of how NaOH concentration, treatment temperature, and treatment time affect the BET surface area of the material, offering insight into their interactive effects, as shown in Fig. 6. The 3D surface plot and corresponding contour map for NaOH concentration and treatment temperature (Fig. 6a, b) reveal that the BET surface area increases significantly with higher treatment temperatures and moderate to high concentrations of NaOH. This suggests that the activation process is highly temperature-dependent, with sufficient chemical interaction at optimal NaOH concentrations enhancing the surface area. However, excessively high concentrations might lead to reduced efficiency due to material degradation or pore collapse. Similarly, the interaction between treatment temperature and treatment time (Fig. 6c, d) shows that a longer duration, when coupled with elevated temperatures, promotes an increase in the BET surface area, but this effect plateaus or decreases beyond certain thresholds, likely due to overexposure leading to pore shrinkage or collapse. The contour plots highlight the regions where these optimal conditions converge, with the red zones marking the combinations of parameters that yield the highest surface area. These results emphasize the critical role of temperature as the most influential parameter, while NaOH concentration and treatment time act as complementary factors that must be carefully adjusted to achieve the desired surface properties.

6. Characterization

6.1. Fourier transform infrared spectroscopy (FTIR)

Fig. 7 shows the FTIR spectra of cellulose before and after the adsorption of Safranin O and Acid Blue 25, providing crucial insights into the functional groups involved in the adsorption mechanism and the extent of interaction between the dye molecules and cellulose. The raw cellulose spectrum exhibits several characteristic absorption bands, with the broad peak at 3299 cm^{-1} corresponding to the O—H stretching vibration, indicative of extensive hydrogen bonding within the cellulose structure [67]. The peak observed at 2897 cm^{-1} is attributed to C—H stretching vibrations from aliphatic groups [68], while the absorption band at 1634 cm^{-1} is assigned to O—H bending [69], often associated with bound water molecules within the cellulose matrix. Additionally, the peaks at 1432 cm^{-1} and 1316 cm^{-1} correspond to C—H bending and C—O stretching vibrations [70], respectively, both of which are characteristic of polysaccharides [71]. The band observed at 890–900 cm^{-1} corresponds to the β-glycosidic linkage (C–O–C) connecting the glucose units in cellulose, indicating the presence of β-1,4 glycosidic bonds that form the linear polymer backbone. The absorption band at 1032 cm^{-1} is

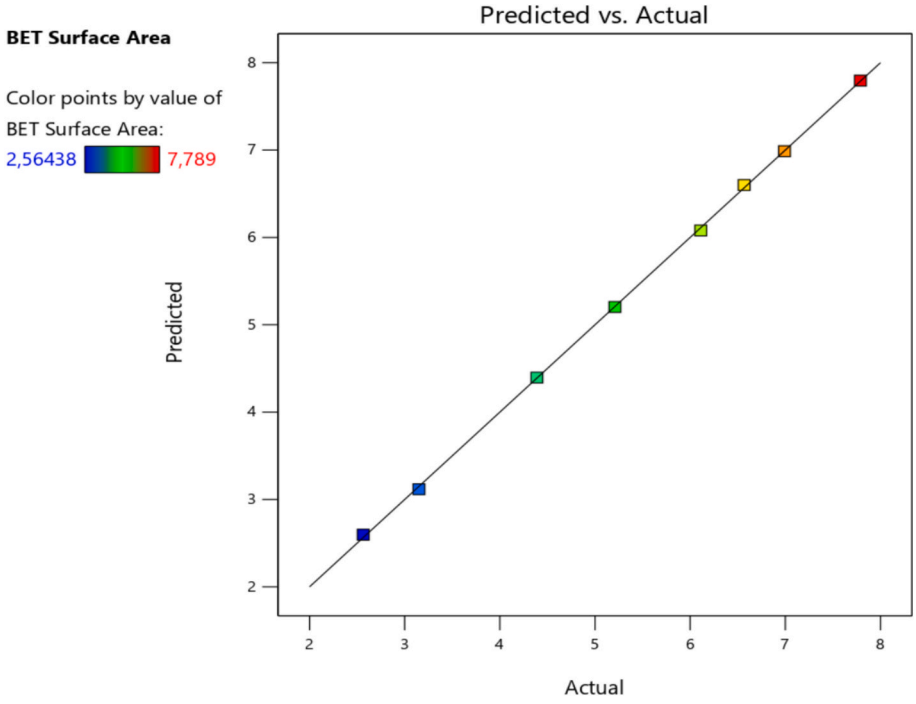

Fig. 4. Correlation between predicted and actual BET surface area values.

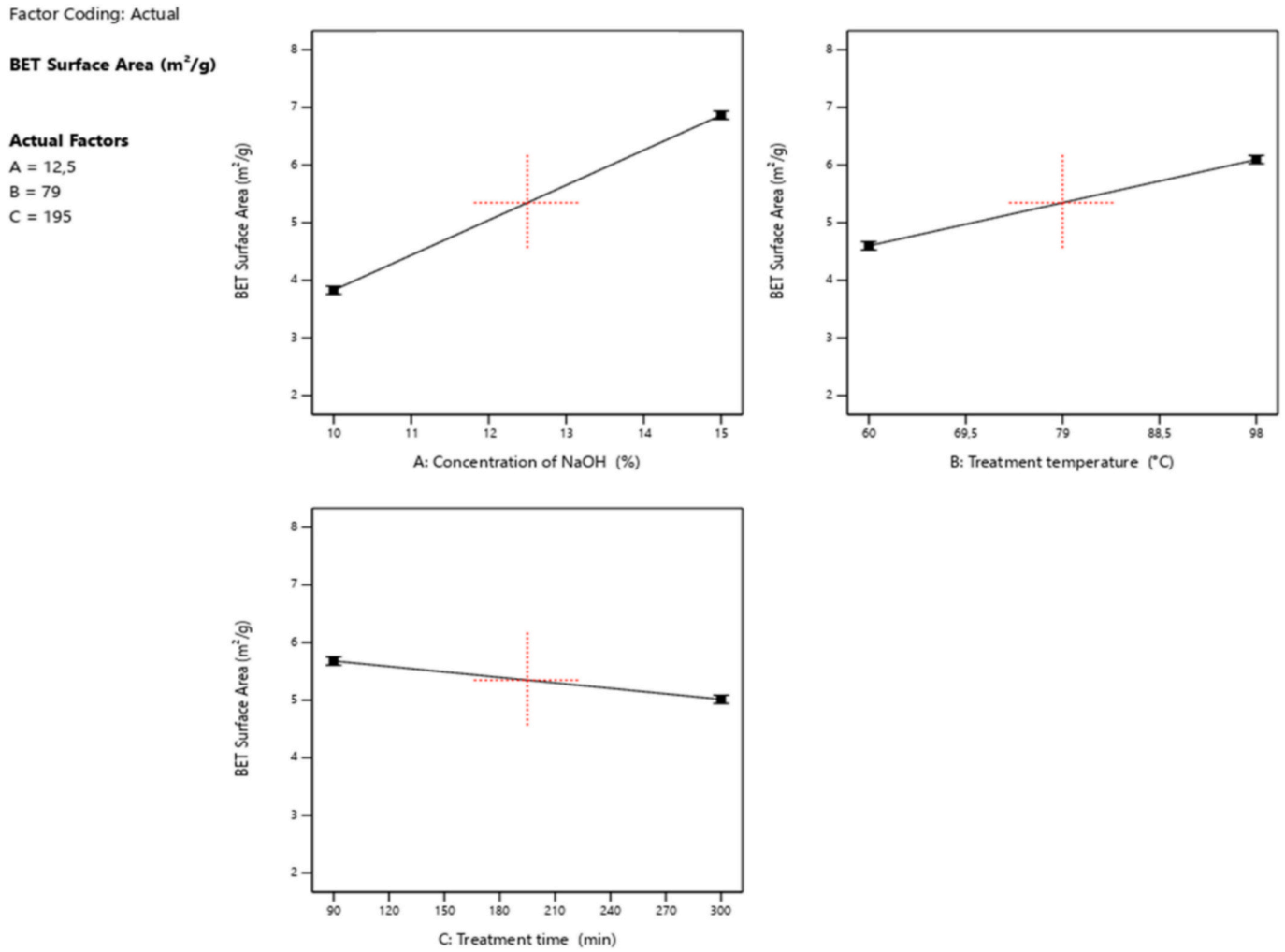

Fig. 5. Main effects of process parameters on BET surface area.

assigned to the C–O–C stretching vibrations within the glucose pyranose rings of the cellulose backbone, reflecting the internal structure of the glucose monomers. Together, these peaks confirm the polymeric nature of cellulose and the typical polysaccharide structure of the material [72]. These two signals confirm the presence of typical polysaccharide structures in the material. Upon adsorption of Safranin O, several spectral changes are observed, suggesting strong interactions between the dye molecules and cellulose functional groups. The O—H stretching vibration undergoes a shift to 3347 cm^{-1}, indicating possible hydrogen bonding interactions between the hydroxyl groups in cellulose and functional groups present in Safranin O. Additionally, the C—H stretching vibration shifts to 2900 cm^{-1}, and new or intensified bands appear at 1635 cm^{-1}, 1436 cm^{-1}, and 1318 cm^{-1}, which can be attributed to interactions involving carboxyl, hydroxyl, and aromatic groups in the dye structure. These modifications indicate that Safranin O forms strong hydrogen bonds with cellulose, possibly facilitated by electrostatic interactions and π-π stacking between the aromatic rings of the dye and the cellulose backbone. In contrast, after adsorption of Acid Blue 25, the O—H stretching band shifts to 3368 cm^{-1}, and the C—H stretching band appears at 2893 cm^{-1}, with relatively weaker intensity changes in comparison to Safranin O. The characteristic peaks at 1645 cm^{-1}, 1425 cm^{-1}, and 1317 cm^{-1} suggest interactions between the dye and cellulose, but their lower intensity and minimal shifts indicate that Acid Blue 25 exhibits weaker binding interactions with cellulose.

6.2. X-ray diffraction (XRD)

Fig. 8 illustrates the X-ray diffraction pattern of the extracted cellulose from Cactus, highlighting distinct peaks at 2θ angles of 11.43°, 16.46°, 22,093°, 24.57° and 37.46°. These diffraction peaks are characteristic of the cellulose Iα and Iβ allomorphs, as well as type II crystalline cellulose [73–75]. Native cellulose typically consists of a mixture of these two crystalline phases, where cellulose Iα exhibits a triclinic unit cell and cellulose Iβ a monoclinic unit cell. The proportion of these allomorphs can vary depending on the origin of the cellulose, Cellulose II is the crystalline phase present in the ordered domains of cellulose resulting from alkaline treatment, as well as in cellulose nanofibers produced through acid hydrolysis [76].

The peak detected at approximately 22° corresponds to the (200) crystallographic plane of cellulose Iβ, which is typically observed near 22.5° [77]. Near this peak, an amorphous phase appears around 2θ = 20.44°, primarily linked to lignin, a key component of the cell wall that contributes significantly to the mechanical strength of wood. The (110) plane of cellulose Iα generates distinct peaks at 16.46°, indicating the presence of cellulose Iα and highlighting the structural differences between the Iα and Iβ allomorphs.

The Segal method, also known as the peak height method, is a widely used analytical technique for evaluating the crystallinity of cellulose samples. This approach determines the crystallinity index (CrI) by comparing the intensity of the diffraction peak associated with crystalline cellulose (I_{ac}) at approximately 2θ = 22.093° to the intensity of the

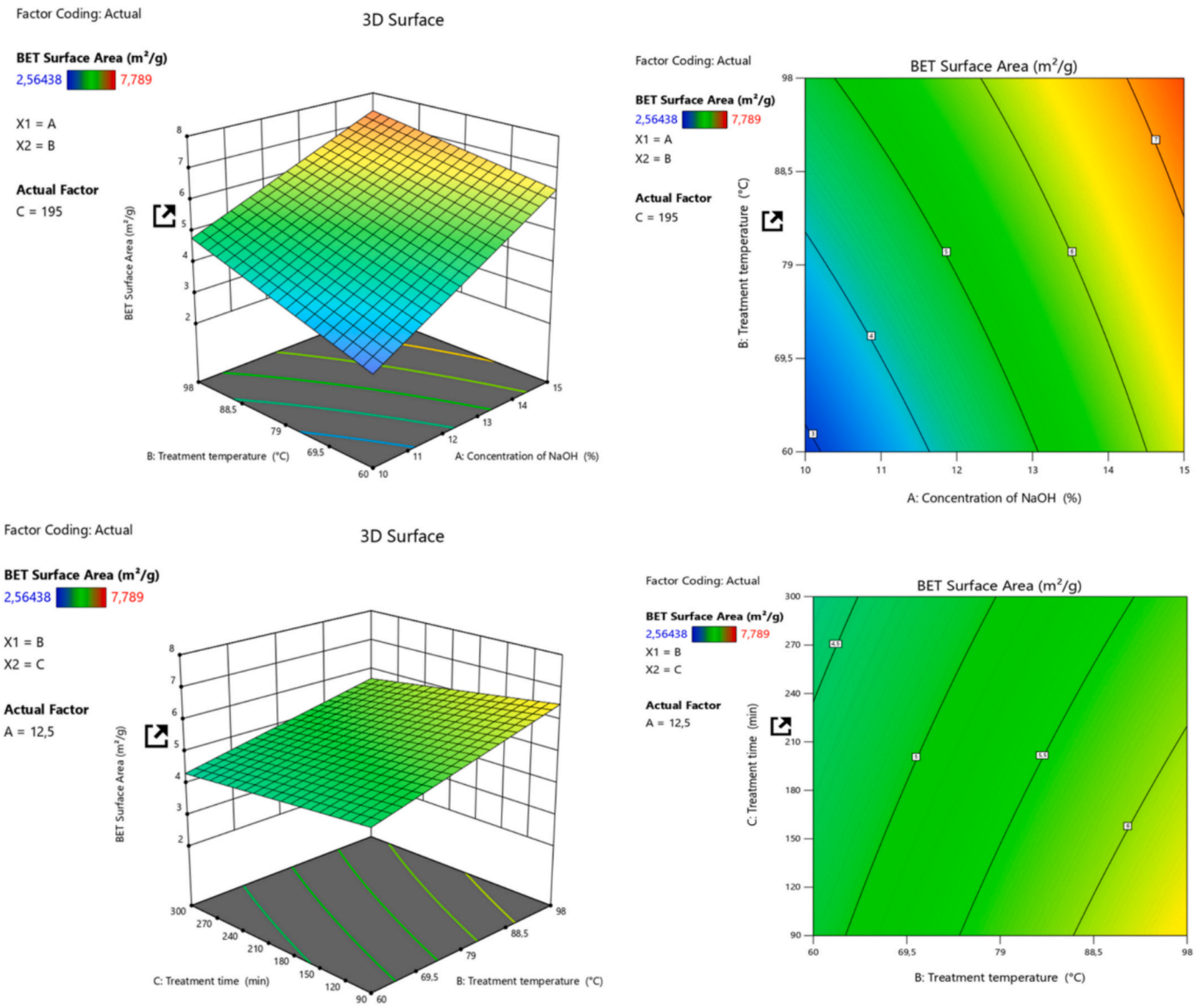

Fig. 6. (a) 3D Response Surface Plot of BET Surface Area vs. NaOH Concentration and Treatment Temperature, (b) Contour Plot of BET Surface Area vs. NaOH Concentration and Treatment Temperature, (c) 3D Response Surface Plot of BET Surface Area vs. Treatment Temperature and Treatment Time, (d) Contour Plot of BET Surface Area vs. Treatment Temperature and Treatment Time.

amorphous phase (I_{am}) at $2\theta = 20.44°$, which corresponds to the lowest intensity in the diffraction pattern. The crystallinity index is calculated using the following Eq. (16):

$$\boldsymbol{CrI}(\%) = \frac{\boldsymbol{I_C - I_{am}}}{\boldsymbol{I_c}} \times \mathbf{100} \tag{16}$$

The average size of the crystal units was determined using the Scherrer equation (Eq. (17)) as described in Table 5. This method relies on the half-value width of the diffraction peaks observed in the X-ray diffraction pattern of the crystalline region. The crystallite size (L_{hkl}) was calculated based on the diffraction pattern data.

$$L_{hkl} = \frac{\boldsymbol{K\lambda}}{\boldsymbol{\beta cos\theta}} \tag{17}$$

where k is the Scherrer constant whose value is 0.94, λ is the wavelength of the X-ray (0.154 nm), β in radians is the total width of the diffraction peak and θ is the corresponding Bragg angle.

6.3. Scanning electron microscopy (SEM)

The SEM micrographs provide a detailed visualization of the morphological changes occurring in cactus-derived cellulose before and after dye adsorption, highlighting the structural modifications induced by the interaction with Acid Blue 25 and Safranin O. The SEM images of raw cellulose (Fig. 9(a)) reveal a highly porous and fibrous structure, characterized by an irregular surface with numerous voids and interconnected networks of cellulose fibers. The rough texture and well-defined fibrillar arrangement suggest a high surface area, which is beneficial for adsorption processes. At higher magnifications (50 μm and 20 μm), the cellulose structure appears loose and open, with distinct pores and crevices that can accommodate dye molecules during the adsorption process. After adsorption of Acid Blue 25 (Fig. 9(b)), the SEM images show significant changes in surface morphology. The initially well-defined porous structure becomes partially covered, indicating the presence of adsorbed dye molecules. The cellulose fibers appear more compact, and the porosity is visibly reduced, suggesting successful interaction between the dye and the cellulose surface. However, even at higher magnifications, some pores and rough areas remain exposed,

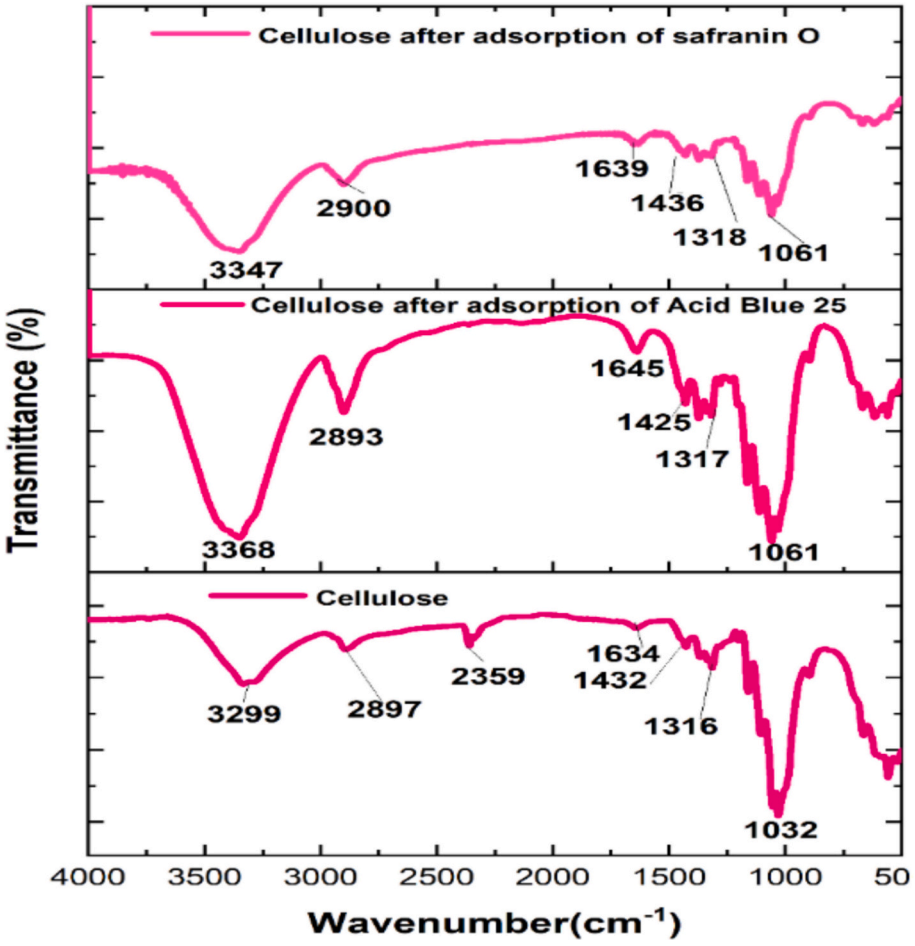

Fig. 7. FTIR spectra of cellulose extracted from cactus before and after the adsorption of Safranin O and Acid Blue 25.

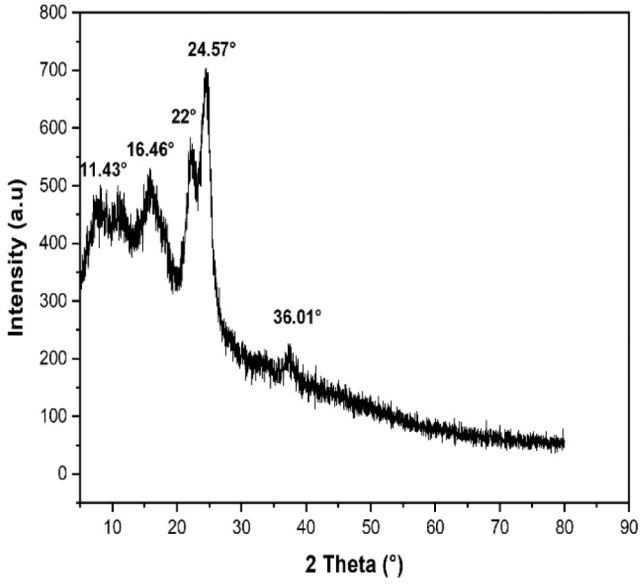

Fig. 8. X-ray diffraction (XRD) patterns of cellulose extracted from cactus.

indicating that Acid Blue 25 does not completely saturate the cellulose surface. This partial coverage suggests that the interaction between Acid Blue 25 and cellulose is moderate, allowing some regions of the material to retain their original texture. In contrast, the SEM micrographs of

Table 5
Peak position, intensity, crystallinity, and lattice parameters.

	Pos. (°2Th)	Height	β (rada)	(%)CrI	L_{hkl} (nm)
1	10.788	163.59264	0.93955		
2	15.769	204.02786	2.39831		
3	22.093	323.91406	1.6642	38.48	0.0938
4	24.575	476.55724	1.98973		0.08
	37.461	115.86088	1.17511		

cellulose after the adsorption of Safranin O (Fig. 9(c)) display more extensive structural modifications, with a significant reduction in porosity. The surface appears much denser and more aggregated, with a nearly complete masking of the fibrillar structure by a thick layer of adsorbed material. At higher magnifications, the cellulose surface is almost entirely coated, with minimal visible pores or voids, indicating a more extensive interaction between Safranin O and cellulose. The compact and layered appearance suggests a strong adherence of Safranin O molecules to the cellulose matrix, leading to a drastic transformation in the material's surface morphology. The observed differences in SEM images confirm that cellulose undergoes notable textural modifications upon dye adsorption, with Safranin O inducing more pronounced structural changes than Acid Blue 25. These micro-structural variations provide clear evidence of the extent of adsorption and demonstrate the ability of cactus-derived cellulose to effectively modify its surface morphology in response to dye uptake.

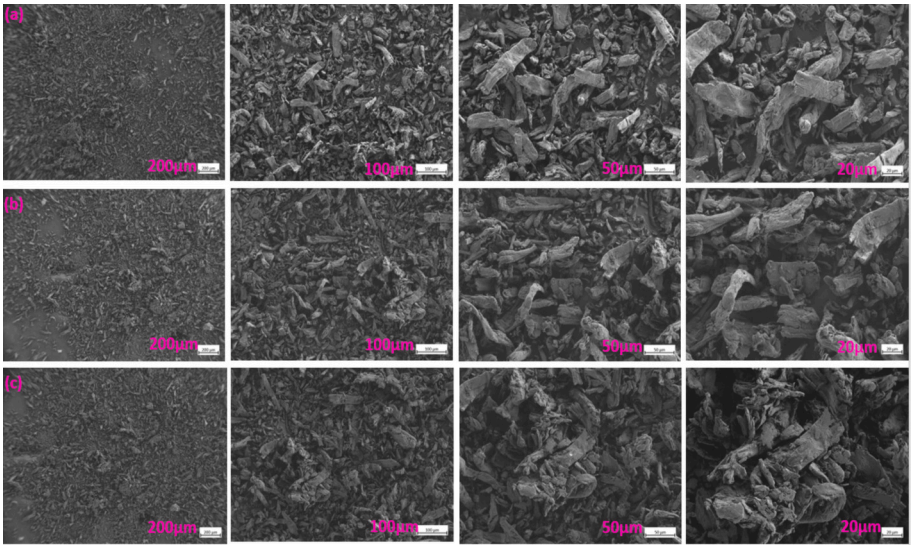

Fig. 9. SEM images of (a) raw cellulose extracted from cactus, (b) cellulose after adsorption of Acid Blue 25, and (c) cellulose after adsorption of Safranin O at different magnifications.

6.4. *Energy dispersive X-ray spectroscopy*

Energy Dispersive X-ray Spectroscopy (EDS) analysis provides insights into the elemental composition of cactus-derived cellulose before and after the adsorption of Acid Blue 25 and Safranin O, revealing significant changes that confirm successful dye uptake. The EDS spectrum of raw cellulose ((Fig. 10(a))) primarily displays peaks corresponding to carbon (C) and oxygen (O), which are characteristic of the organic nature of cellulose [78]. The high carbon content is attributed to the polysaccharide backbone of cellulose [79], while oxygen originates from hydroxyl (-OH) and ether (-O-) functional groups present in the cellulose structure [80]. The uniform distribution of these elements suggests a clean and unmodified cellulose surface, providing a reference for comparison after dye adsorption.

After the adsorption of Acid Blue 25 (Fig. 10(b)), the EDS spectrum exhibits notable changes, particularly with an increase in nitrogen (N) content. This increase is attributed to the presence of nitrogen-containing functional groups in the Acid Blue 25 dye molecules. Additionally, the oxygen content slightly increases, which could be due to interactions between the dye's sulfonate ($-SO_3^-$) groups and the

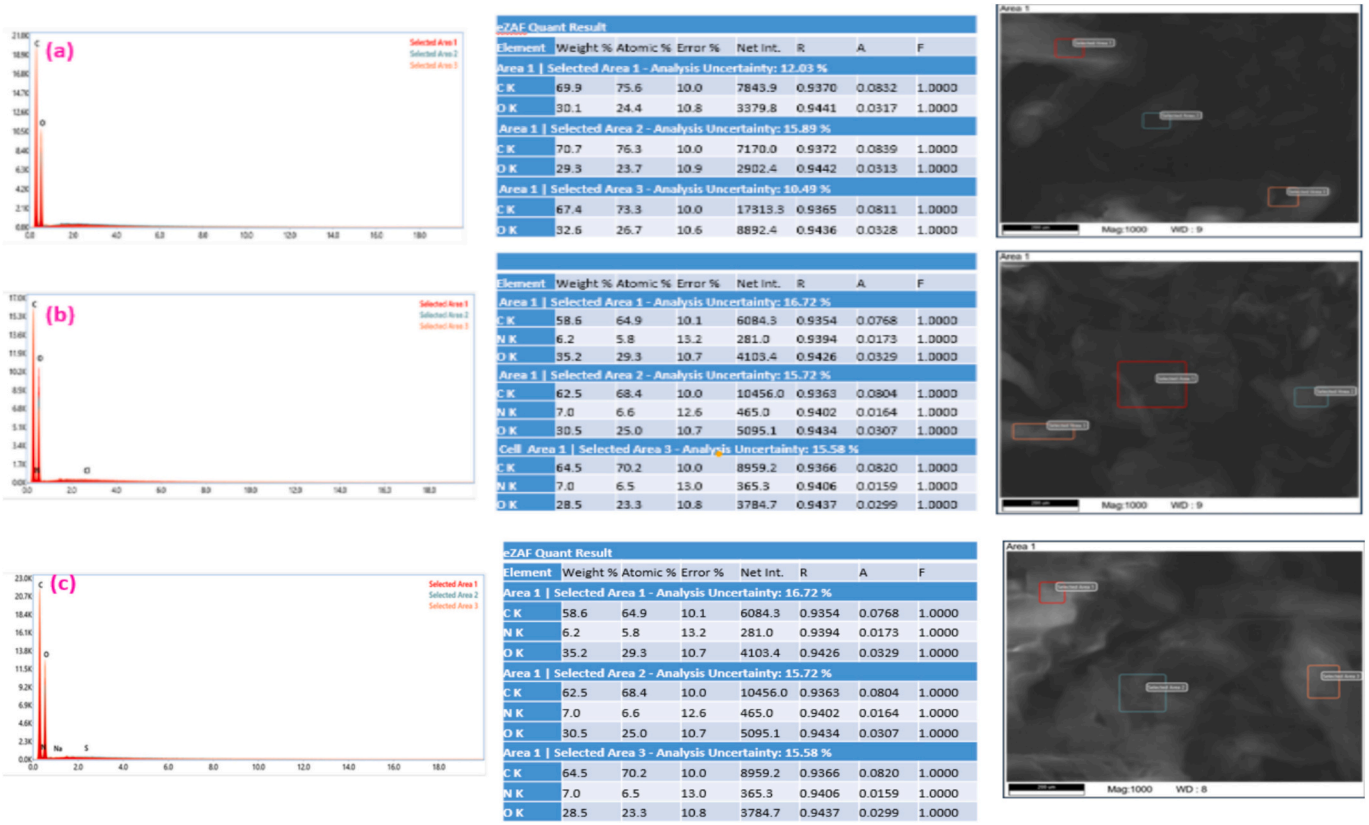

Fig. 10. EDS images of (a) cellulose extracted from cactus, (b) cellulose after adsorption of Acid Blue 25, and (c) cellulose after adsorption of Safranin O.

cellulose hydroxyl groups. The carbon content remains relatively stable, but the adsorption process leads to a slight redistribution of elements, as observed in the selected area analysis. These variations in elemental composition confirm that Acid Blue 25 has successfully interacted with the cellulose surface, though some regions remain unchanged, indicating moderate adsorption. In contrast, the EDS spectrum of cellulose after Safranin O adsorption (Fig. 10(c)) reveals even more pronounced changes in elemental composition. A significant increase in nitrogen content is observed, which is consistent with the molecular structure of Safranin O, a cationic dye that contains multiple nitrogen atoms. The increase in nitrogen concentration suggests strong adsorption of Safranin O onto the cellulose surface. The carbon content remains relatively unchanged, while oxygen levels slightly fluctuate, indicating possible interactions between the dye molecules and cellulose functional groups. Compared to Acid Blue 25, the higher nitrogen signal suggests that Safranin O has a stronger affinity for cellulose, likely due to electrostatic interactions and hydrogen bonding. The uniform distribution of nitrogen throughout the analyzed areas further supports the conclusion that the adsorption of Safranin O is more extensive than that of Acid Blue 25.

7. Adsorption

The adsorption behavior of Acid Blue 25 and Safranin O onto cellulose was systematically evaluated under varying conditions, including contact time, adsorbent mass, solution pH, and initial dye concentration (C_0). Each of these parameters played a crucial role in determining the removal efficiency of the dyes, revealing the distinct interaction mechanisms governing their adsorption onto the cellulose surface.

7.1. Effect of contact time on the adsorption of Acid Blue 25 and Safranin O

The effect of contact time revealed a distinct biphasic adsorption behavior for both dyes, highlighting the dynamic nature of their interaction with the cellulose surface, as shown in Fig. 11(a). During the initial phase of adsorption, a rapid uptake of dye molecules was observed, primarily due to the abundance of available active sites on the cellulose surface [81]. At this stage, dye molecules could easily access these sites without significant competition, resulting in a high initial adsorption rate [82]. However, as the process progressed, the adsorption rate gradually declined, eventually reaching equilibrium [83]. This decrease in adsorption rate can be attributed to the progressive saturation of active sites, steric hindrance from already adsorbed dye molecules, and potential repulsive forces between similarly charged species [84]. For Acid Blue 25, the optimal contact time was found to be 130 min, achieving a maximum removal efficiency of 41.12 %. The relatively slow adsorption process suggests that the interactions between Acid Blue 25 and the cellulose surface were weaker compared to th ose of Safranin O. Given that Acid Blue 25 is an anionic dye, its adsorption onto cellulose, which carries a negative charge at higher pH values, is not predominantly governed by electrostatic attraction. Instead, other weaker forces, such as hydrogen bonding and van der Waals interactions, play a more significant role. Additionally, diffusion limitations may have contributed to the slower adsorption kinetics, as dye molecules must navigate through the porous cellulose structure to reach available binding sites [85]. In contrast, Safranin O exhibited a much faster adsorption process, achieving its highest removal efficiency of 91.98 % within just 90 min. This rapid adsorption can be attributed to the strong electrostatic attraction between the cationic Safranin O molecules and the negatively charged cellulose surface at higher pH levels. The positively charged dye molecules are readily attracted to the negatively

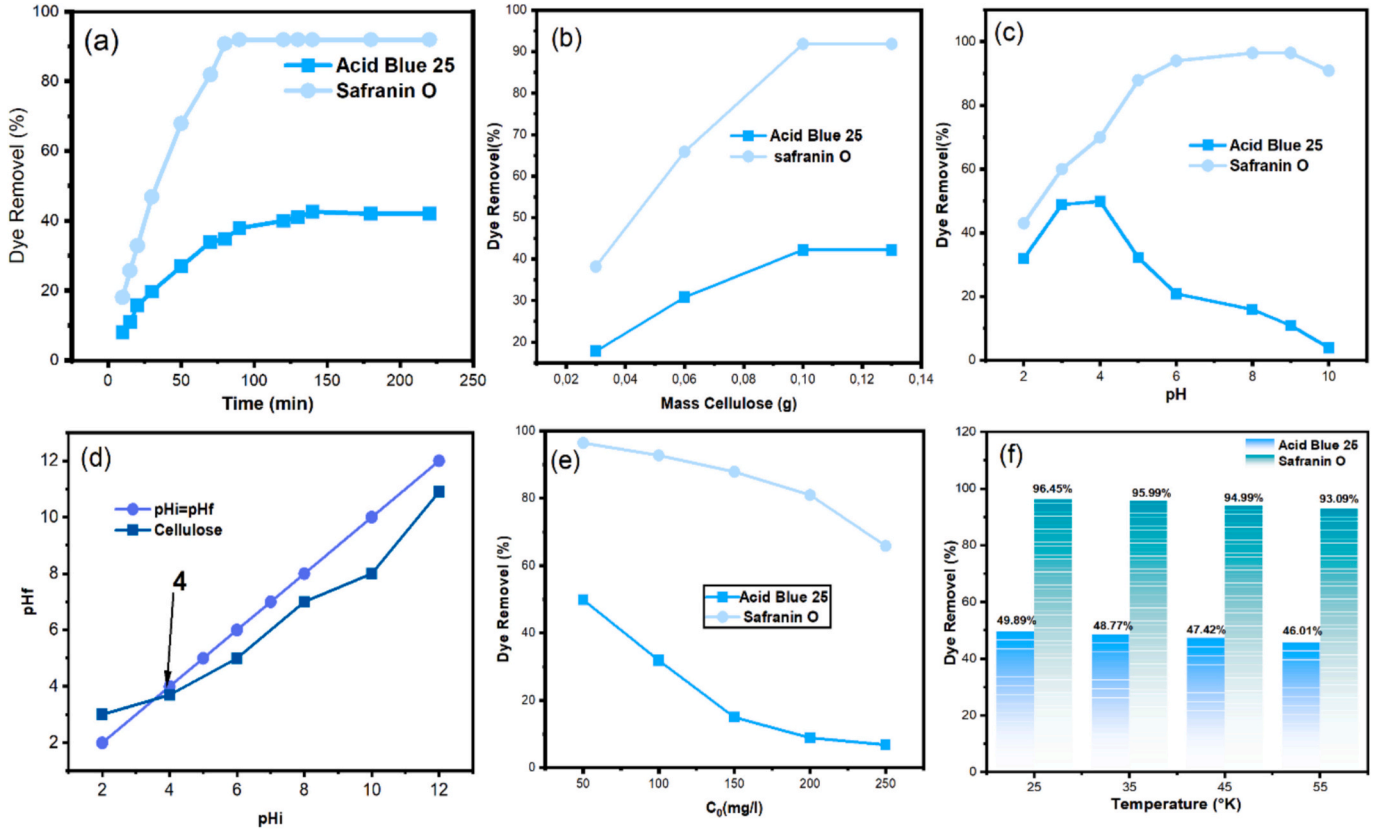

Fig. 11. Effect of various parameters on the removal of Acid Blue 25 and Safranin O using cellulose, (a) contact time (b) adsorbent dose (mass of cellulose), (c) pH, (d) pHzc (e) initial dye concentration, (f) temperature.

charged hydroxyl (-OH) and other functional groups on cellulose, facilitating efficient adsorption. Furthermore, hydrogen bonding interactions between Safranin O and cellulose's hydroxyl groups further enhance the adsorption process. Unlike Acid Blue 25, which relies on weaker and non-electrostatic interactions, Safranin O benefits from a more favorable binding mechanism, resulting in higher removal efficiency and faster equilibrium attainment.

7.2. Effect of mass on the adsorption of Acid Blue 25 and Safranin O

The effect of adsorbent mass illustrated in Fig. 11(b) further highlighted the distinct adsorption behaviors of Acid Blue 25 and Safranin O, emphasizing the role of active site availability and interaction mechanisms in determining removal efficiency [86]. Increasing the adsorbent mass generally leads to a greater number of available adsorption sites, enhancing the removal of dye molecules from the solution [87]. However, the extent to which adsorption efficiency improves varies depending on the nature of the dye and its interaction with the cellulose surface [88]. For Acid Blue 25, the optimal adsorbent mass was found to be 0.1 g, achieving an impressive removal efficiency of 91.88 %. This high efficiency can be attributed to the increased availability of active sites and the expanded surface area of cellulose, allowing for greater dye adsorption [89]. At lower adsorbent masses, the limited number of active sites may not be sufficient to accommodate all the dye molecules in solution, resulting in lower removal efficiency [90]. As the adsorbent mass increases, more binding sites become available, enabling higher dye uptake and improved adsorption performance [91]. However, beyond the optimal mass, further increases in adsorbent dosage may not significantly enhance removal efficiency, as most of the dye molecules would already be adsorbed, leading to equilibrium saturation [92]. In contrast, Safranin O exhibited a different adsorption trend, with a maximum removal efficiency of only 42.22 % at the same adsorbent mass of 0.1 g. This comparatively lower efficiency suggests that the adsorption process for Safranin O may be limited by site accessibility rather than the total number of available active sites. Unlike Acid Blue 25, which benefits from increased adsorbent dosage, Safranin O's adsorption may be constrained by steric hindrance, saturation effects, or differences in binding affinity. The positively charged Safranin O molecules may experience stronger competition for available sites, leading to reduced adsorption efficiency despite an increase in adsorbent mass [23]. Additionally, the presence of excess cellulose particles in the solution could lead to partial aggregation, potentially reducing the overall effective surface area available for adsorption.

7.3. Point of Zero Charge (pHzc) and effect of pH on the adsorption of Acid Blue 25 and Safranin O

The pH of the solution plays a fundamental role in governing the adsorption efficiency, as it simultaneously affects the surface charge of the cellulose and the ionization state of the dye molecules, as shown in Fig. 11(c). This dual influence is critical because it dictates the nature, strength, and type of interactions between the adsorbent and the adsorbate, including electrostatic attraction or repulsion, hydrogen bonding, and van der Waals forces. The point of zero charge (pH_pzc) of the cactus-derived cellulose was determined to be 4 (Fig. 8d), indicating that at pH values below 4, the cellulose surface carries a net positive charge, while at pH values above 4, it becomes increasingly negatively charged. This surface charge variation has a significant effect on the adsorption of dyes with differing ionic characteristics.

Acid Blue 25, an anionic dye, has a pKa value of approximately 4.7, which means that at pH values below its pKa, a substantial fraction of the dye molecules are protonated and less negatively charged, whereas above this pH, the dye exists predominantly in its deprotonated, negatively charged form. In our experiments, the most favorable adsorption of Acid Blue 25 occurred at pH 4, where the cellulose surface is near neutral, minimizing electrostatic repulsion between the dye and the adsorbent. At this pH, the adsorption process was primarily driven by secondary forces such as hydrogen bonding and van der Waals interactions rather than strong electrostatic attraction, resulting in a removal efficiency of 49.89 %. At pH values significantly below 4, the cellulose surface carries a stronger positive charge, which could in theory favor interaction with the anionic fraction of the dye; however, the limited ionization of the dye and possible competitive protonation effects reduce adsorption. Conversely, at pH values above the dye's pKa, the cellulose surface is negatively charged, and hydroxyl ions (OH^-) in the solution compete with the anionic Acid Blue 25 molecules for active sites on the cellulose, leading to a decrease in adsorption efficiency. This indicates that both the dye ionization state and electrostatic interactions are critical in controlling adsorption.

In contrast, Safranin O is a cationic dye with a pKa value of approximately 6.4. Its adsorption behavior is almost entirely governed by electrostatic interactions with the cellulose surface. The highest removal efficiency of 96.44 % was observed at pH 9, where the cellulose surface is strongly negatively charged. In this scenario, electrostatic attraction between the positively charged dye molecules and the negatively charged cellulose surface dominates the adsorption process, significantly enhancing retention. At lower pH values, where the cellulose surface carries a positive charge, electrostatic repulsion hinders adsorption, leading to a marked reduction in dye removal. In addition to electrostatic effects, hydrogen bonding and van der Waals interactions also contribute to Safranin O adsorption, particularly at pH values close to its pKa, where partial ionization occurs.

Overall, the adsorption behavior of both dyes demonstrates the importance of considering the pKa values in combination with the pH_pzc of the adsorbent. For Acid Blue 25, optimal adsorption occurs when repulsive forces are minimized and secondary interactions dominate, whereas for Safranin O, adsorption is maximized when strong electrostatic attraction is present. These results highlight that the interplay between the solution pH, the cellulose surface charge, and the dye ionization state is a key factor controlling adsorption efficiency. Understanding these interactions allows for the optimization of pH conditions to achieve maximum dye removal and provides insight into the mechanisms underlying selective adsorption of different ionic dyes on cellulose surfaces.

7.4. Effect of initial concentration on the adsorption of Acid Blue 25 and Safranin O

The effect of initial dye concentration (C_o) on adsorption efficiency closely aligned with the saturation phenomenon observed during the contact time studies [92]. Fig. 11(e) shows that as the initial dye concentration increased, the removal efficiency for both dyes exhibited a noticeable decline. This behavior can be attributed to the finite number of active adsorption sites available on the cellulose surface, which become increasingly saturated as more dye molecules compete for adsorption at higher concentrations [93]. At lower C_o values, the active sites are more readily accessible, allowing for higher removal efficiency. However, as C_o increases, the surface coverage of the adsorbent reaches its capacity, limiting the extent of further adsorption [94]. This trend was particularly pronounced for Acid Blue 25, which demonstrated a steeper decline in removal efficiency with increasing initial concentration. The weaker interactions between Acid Blue 25 and cellulose, likely dominated by van der Waals forces and hydrogen bonding, contributed to this effect [95]. As the number of dye molecules in solution increased, the competition for available binding sites intensified, leading to a significant reduction in adsorption performance [96]. In contrast, while Safranin O also exhibited a decline in removal efficiency with increasing C_o, its overall adsorption efficiency remained higher throughout the concentration range studied. This can be attributed to the stronger electrostatic interactions between Safranin O and the cellulose surface, which facilitated more effective dye adsorption even at higher concentrations [97]. The positively charged nature of Safranin O likely

enhanced its affinity toward the negatively charged functional groups on cellulose, resulting in a more favorable adsorption process. Consequently, despite the general trend of decreasing removal efficiency with increasing dye concentration, the impact was less severe for Safranin O compared to Acid Blue 25 [98].

7.5. Effect of temperature on the adsorption of Acid Blue 25 and Safranin O

The effect of temperature on the removal efficiency of Safranin O and Acid Blue 25 is shown in Fig. 11(f). The removal efficiency of Acid Blue 25 remains significantly higher compared to Safranin O across all tested temperatures (25 K to 55 K). Acid Blue 25 shows consistently high removal rates, ranging from 96.45 % at 25 K to 93.09 % at 55 K, indicating a relatively stable adsorption performance. In contrast, Safranin O demonstrates lower removal efficiency, decreasing slightly from 49.89 % at 25 K to 46.01 % at 55 K. This decline suggests that the adsorption process for Safranin O may be more sensitive to increasing temperature, possibly due to reduced interaction strength or competition for active sites.

7.6. Modeling of adsorption kinetic

The adsorption kinetics of Acid Blue 25 and Safranin O were analyzed using two widely recognized models: the Pseudo-First-Order (PFO) and the Pseudo-Second-Order (PSO) models, as shown in Table 6 and Fig. 12(a), (b), (c), and (d). For the PFO model [99], the calculated equilibrium adsorption capacities (qe,cal) were found to be 25.23 mg/g for Acid Blue 25 and 88.23 mg/g for Safranin O, indicating that the initial adsorption capacity for Safranin O was significantly higher than for Acid Blue 25. The rate constant (k_1), which reflects the adsorption rate, was 0.02748 min^{-1} for Acid Blue 25 and 0.0504 min^{-1} for Safranin O. The PFO model showed a good correlation for Acid Blue 25, with a correlation coefficient (R^2) of 0.979, but the fit was relatively weaker for Safranin O, with an R^2 value of 0.853, suggesting that the PFO model was not as effective in describing the adsorption of Safranin O. In contrast, the PSO model [100], which is more appropriate for describing adsorption processes that occur on a surface with limited adsorption sites, provided improved results. The calculated equilibrium adsorption capacities (qe, cal) were 31.39 mg/g for Acid Blue 25 and 105.04 mg/g for Safranin O, both of which were higher than those predicted by the PFO model, suggesting that the adsorption of both dyes followed a second-order kinetic process more closely. The rate constants (k_2) were 0.000492 g. $mg^{-1}.min^{-1}$ for Acid Blue 25 and 0.0000823 g. $mg^{-1}.min^{-1}$ for Safranin O, which are relatively small and indicate slower adsorption processes. Notably, the PSO model demonstrated a significantly better fit to the experimental data, with R^2 values of 0.990 for Acid Blue 25 and 0.995 for Safranin O, indicating that the adsorption processes for both dyes were more accurately described by the second-order model. These results underscore the importance of using the PSO model to describe the adsorption kinetics of Acid Blue 25 and Safranin O, as it provides a more accurate representation of the dye removal process, particularly for Safranin O, where the PFO model exhibited a weaker fit.

Table 6
Kinetic parameters for the adsorption of Acid Blue 25 and Safranin O: Pseudo First Order (PFO) and Pseudo Second Order (PSO) models.

Model	Parameter	Acid Blue 25	Safranin O
Pseudo First Order (PFO)	$q_{e,cal}$ (mg/g)	25.23	88.23
	k_1 (min^{-1})	0.02748	0.0504
	R^2	0.979	0.853
Pseudo Second Order (PSO)	$q_{e,cal}$ (mg/g)	31.39	105.04
	k_2 ($g.mg^{-1}.min^{-1}$)	0.000492	0.0000823
	R^2	0.990	0.995

7.7. Modeling of adsorption isotherms

The adsorption of Acid Blue 25 and Safranin O was modeled using three well-known adsorption isotherms: Langmuir, Freundlich, and Temkin, to analyze the equilibrium data and understand the nature of the adsorption process for each dye In the case of the Langmuir isotherm model, as shown in Table 7 and Fig. 12(e) and (f), which assumes a monolayer adsorption on a surface with a fixed number of adsorption sites, the maximum adsorption capacity (qm) for Acid Blue 25 was found to be 11.07 mg/g, whereas for Safranin O, it was significantly higher at 124.38 mg/g. This indicates that Safranin O has a much higher adsorption capacity on the surface compared to Acid Blue 25. The Langmuir constant (K_L), which reflects the affinity between the adsorbate and the adsorbent [31], was 0.417 L/mg for Acid Blue 25 and 27.40 L/mg for Safranin O. The high value of K_L for Safranin O suggests a stronger affinity and a more favorable adsorption process for this dye. The Langmuir model exhibited a strong fit to the experimental data, with correlation coefficients (R^2) of 0.984 for Acid Blue 25 and 0.997 for Safranin O. These high R^2 values indicate that the adsorption of both dyes follows the characteristics of monolayer adsorption, with the dye molecules occupying identical sites on the surface without further interaction. For the Freundlich isotherm, as shown in Table 7 and Fig. 12 (g) and (h), which is based on the assumption of adsorption on a heterogeneous surface, the Freundlich constant (K_F) for Acid Blue 25 was 83.93 mg/g indicating a higher initial adsorption capacity compared to Safranin O, which had a K_F value of 42.11 mg/g. The parameter $1/n_F$ is used to assess the adsorption intensity and heterogeneity of the adsorption sites. For Acid Blue 25, 1/nF was 2.87, while for Safranin O, it was 3.98. These values indicate that the adsorption process for both dyes occurs on heterogeneous surfaces, but with greater intensity for Acid Blue 25. The correlation coefficients (R^2) for the Freundlich model were 0.89 for Acid Blue 25 and 0.95 for Safranin O, showing that while the Freundlich model is applicable to the data, it provides a moderate fit compared to the Langmuir model, especially for Acid Blue 25. The Temkin model, as shown in Table 7 and Fig. 12(i) and (j), which assumes that the heat of adsorption decreases linearly as the adsorption sites become occupied, showed a reasonable fit for both dyes. The Temkin constant (B_T) for Acid Blue 25 was 6.27 J/mol, while for Safranin O, it was 19.88 J/mol, indicating different adsorption energies for the two dyes. A higher BT value for Safranin O suggests stronger binding energy during adsorption. The Temkin constant (K_T), which reflects the adsorption equilibrium, was found to be 0.0006 L/mg for Acid Blue 25 and 5.69 L/mg for Safranin O. The high value of K_T for Safranin O indicates a stronger tendency for adsorption at higher concentrations. The correlation coefficients (R^2) for the Temkin model were 0.921 for Acid Blue 25 and 0.950 for Safranin O, indicating that the Temkin model is also reasonably suitable for describing the adsorption data for both dyes, though it does not provide as good a fit as the Langmuir model.

7.8. Thermodynamic study

The thermodynamic parameters for the adsorption of Acid Blue 25 and Safranin O were evaluated to understand the nature of the adsorption process at different temperatures, as presented in Table 8 and Fig. 12(k) and (l). The change in enthalpy (ΔH°) for Acid Blue 25 was −4.195 kJ/mol, indicating that the adsorption process is exothermic and releases heat. In comparison, Safranin O exhibited a more negative ΔH° of −20.45 kJ/mol, suggesting a significantly stronger exothermic adsorption process. The entropy change (ΔS°) for Acid Blue 25 was −17.18 J/mol·K, indicating a decrease in randomness and the formation of a more ordered system during adsorption. Safranin O showed a more negative ΔS° of −43.46 J/mol·K, further reflecting a highly ordered adsorption mechanism.

The Gibbs free energy change (ΔG°), which reflects the spontaneity of the adsorption process, was calculated at 298 K, 308 K, and 318 K. For Acid Blue 25, ΔG° values were positive at all temperatures, specifically

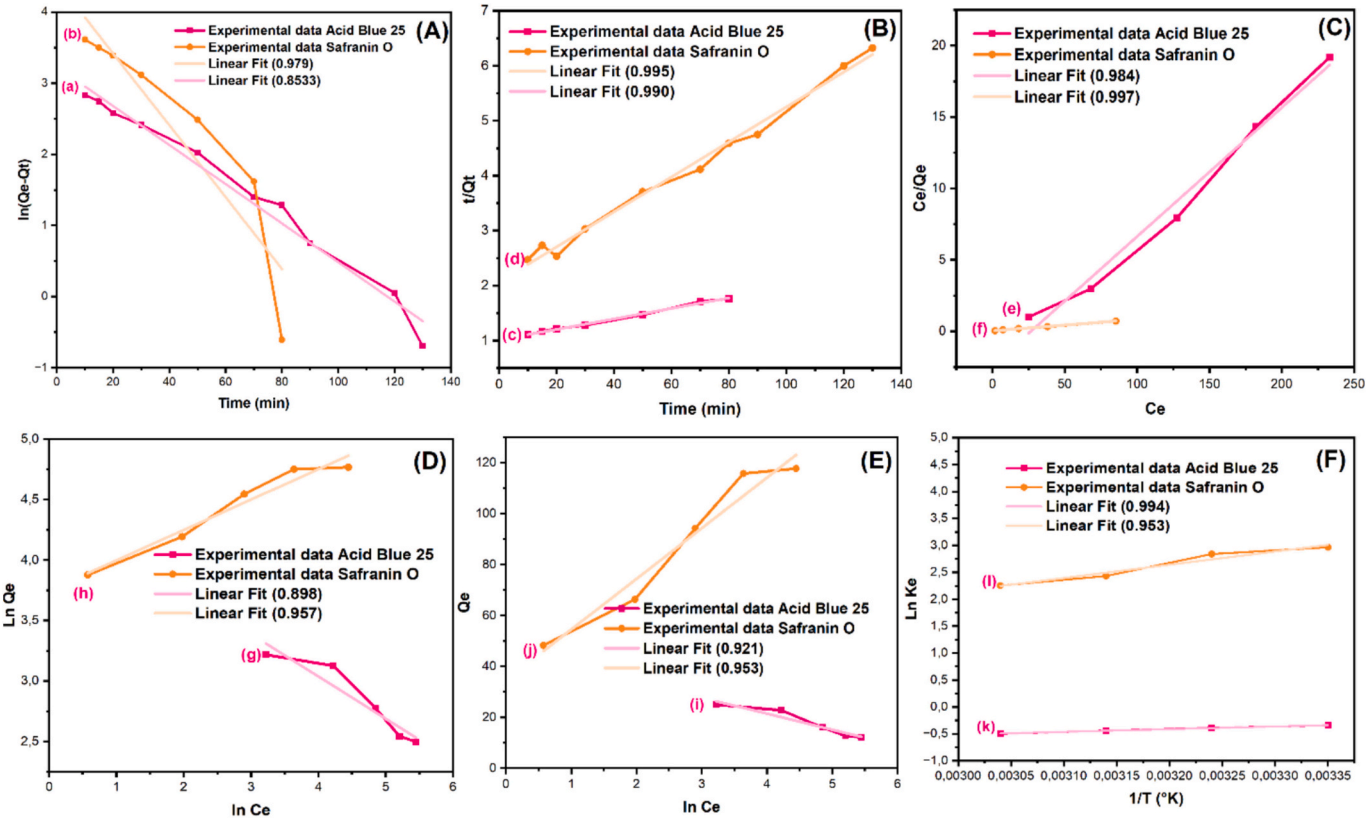

Fig. 12. A: (a) Pseudo-First-Order Kinetic Model for Acid Blue 25, (b) Pseudo-First Order Kinetic Model for Safranin O. B: (c) Pseudo-Second-Order Kinetic Model for Acid Blue 25, (d) Pseudo-Second-Order Kinetic Model for Safranin O. C: (e) Langmuir Isotherm Model for Acid Blue 25, (f) Langmuir Isotherm Model for Safranin O. D: (g) Freundlich Isotherm Model for Acid Blue 25, (h) Freundlich Isotherm Model for Safranin O. E: (i) Temkin Isotherm Model for Acid Blue 25, (j) Temkin Isotherm Model for Safranin O. F: (k) Van't Hoff Plot for Thermodynamic Analysis of Safranin O Adsorption, (l) Van't Hoff Plot for Thermodynamic Analysis of Acid Blue 25 Adsorption.

Table 7
Adsorption isotherm parameters for Acid Blue 25 and Safranin O: Langmuir, Freundlich, and Temkin models.

Model	Parameter	Acid Blue 25	Safranin O
Langmuir	qm (mg/g)	11.07	124.38
	K_L (L/mg)	0.417	27.40
	R^2	0.984	0.997
Freundlich	K_F (mg/g)	83.93	42.11
	1/nF	2.87	3.98
	R^2	0.89	0.95
Temkin	B_T (J/mol)	6.27	19.88
	K_T (L/mg)	0.0006	5.69
	R^2	0.921	0.950

Table 8
Thermodynamic parameters for the adsorption of Acid Blue 25 and Safranin O: Enthalpy (ΔH°), Entropy (ΔS°), and Gibbs Free Energy (ΔG°) at different temperatures.

Adsorbents	ΔH∘ (kJ/mol)	ΔS∘ (J/mol·K)	ΔG ∘ at 298 K (kJ/mol)	ΔG ∘ at 308 K (kJ/mol)	ΔG∘ at 318 K (kJ/mol)
Acid Blue 25	−4.195	−17.18	1.92	2.09	2.26
Safranin O	−20.45	−43.46	−7.54	−7.10	−6.66

1.92 kJ/mol at 298 K, 2.09 kJ/mol at 308 K, and 2.26 kJ/mol at 318 K, indicating that the adsorption of Acid Blue 25 is not thermodynamically favorable under the studied conditions. In contrast, Safranin O adsorption was spontaneous, with negative ΔG° values of −7.54 kJ/mol at 298 K, −7.10 kJ/mol at 308 K, and −6.66 kJ/mol at 318 K. These results indicate that the adsorption of Safranin O is both exothermic and spontaneous, although it becomes slightly less favorable as the temperature increases.

8. DFT analysis

8.1. Global reactivity descriptions

The molecular orbital analysis provides crucial insights into the electronic properties and adsorption behavior of Acid-Blue 25 and Safranin O onto cellulose. The energy levels of the Highest Occupied Molecular Orbital (HOMO) and Lowest Unoccupied Molecular Orbital (LUMO), along with the energy gap (Eg), reveal significant differences in the adsorption efficiency of these dyes [101,102]. As indicated in Table 9 and Fig. 13, cellulose (Fig. 13c) exhibits a large energy gap of 6.38 eV, with a HOMO energy of −6.86 eV and a LUMO energy of −0.48 eV, confirming its electronic stability and limited inherent reactivity. The dye molecules, however, display significantly lower energy gaps,

Table 9
Electronic properties (HOMO, LUMO, and Band Gap) of cellulose, Acid Blue 25, Safranin O, and their complexes.

Name of the molecules	HOMO (eV)	LUMO (eV)	Eg (eV)
Cellulose	−6.86	−0.48	6.38
Acid-Blue 25	−5.33	−3.11	2.22
Safranin O	−4.25	−2.55	1.70
Cellulose@Acid-Blue 25	−5.79	−3.46	2.33
Cellulose@Safranin O	−5.65	−2.95	2.70

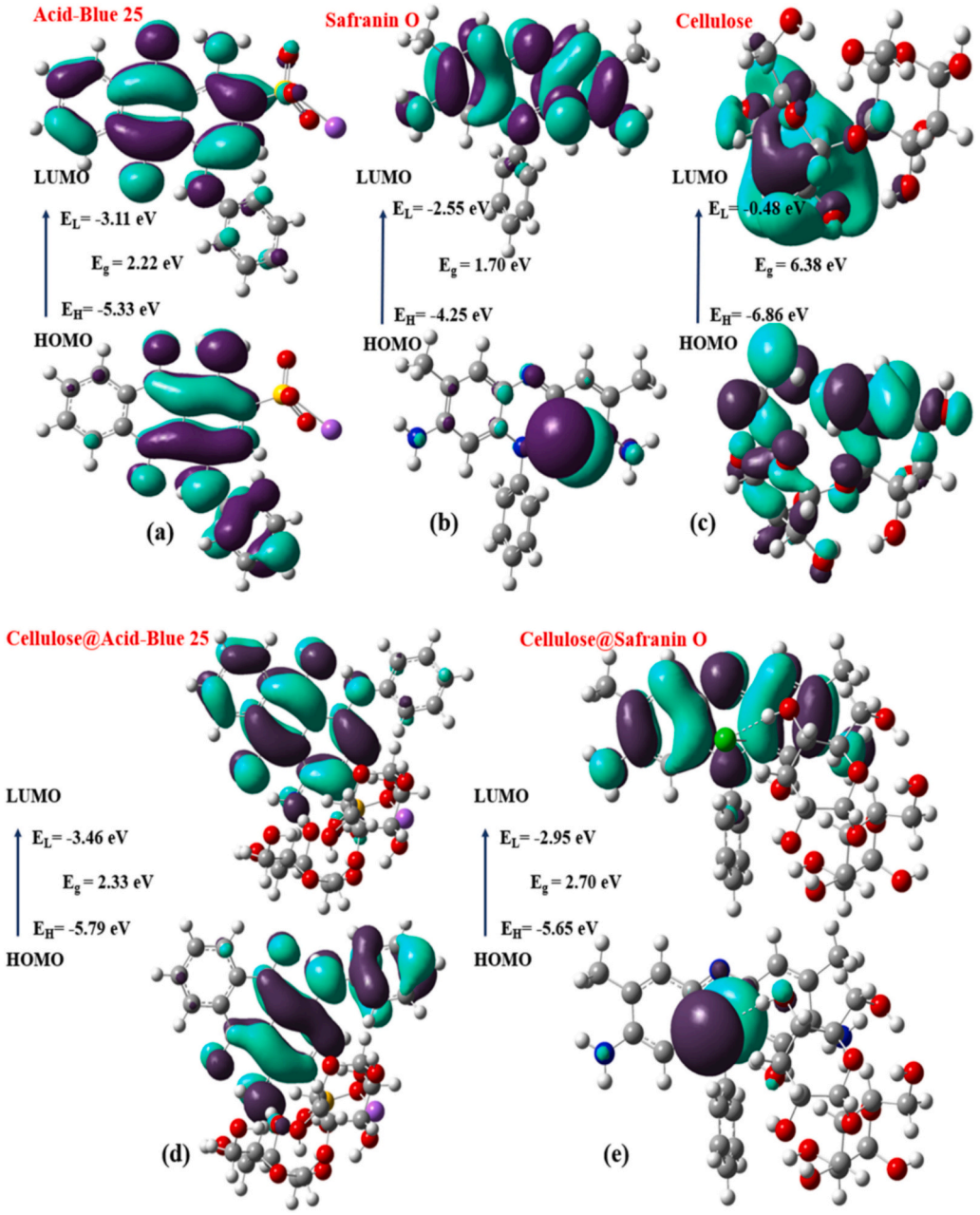

Fig. 13. Frontier Molecular Orbitals (HOMO-LUMO) and Energy Gaps of (a) Acid Blue 25, (b) Safranin O, (c) Cellulose, (d) Cellulose@Acid Blue 25, (e) Cellulose@Safranin O.

suggesting their higher reactivity and propensity to interact with cellulose. Acid-Blue 25 (Fig. 13a) has a HOMO level of −5.33 eV, a LUMO level of −3.11 eV, and a relatively small energy gap of 2.22 eV, whereas Safranin O (Fig. 103b) has a HOMO at −4.25 eV, a LUMO at −2.55 eV, and an even smaller energy gap of 1.70 eV. The lower energy gap of Safranin O compared to Acid-Blue 25 suggests that it is more chemically reactive, facilitating stronger electronic interactions with the cellulose surface. Upon adsorption onto cellulose, both dyes undergo notable electronic modifications, reflected in changes to their HOMO, LUMO, and energy gap values. The Cellulose@Acid-Blue 25(Fig. 13d) complex exhibits an energy gap of 2.33 eV (compared to 2.22 eV for free Acid-Blue 25), while the Cellulose@Safranin O (Fig. 13e) complex shows an energy gap of 2.70 eV (compared to 1.70 eV for free Safranin O). Interestingly, despite the increase in the energy gap upon adsorption, Safranin O exhibits stronger adsorption onto cellulose compared to Acid-Blue 25. This can be attributed to multiple factors. First, the higher HOMO energy of Safranin O (−4.25 eV) compared to Acid-Blue 25 (−5.33 eV) means that Safranin O has a greater ability to donate electrons, facilitating stronger interactions with the cellulose functional groups, particularly through electrostatic and π-π stacking interactions. Additionally, the molecular structure of Safranin O, with its planar aromatic rings and nitrogen-containing groups, enhances its affinity for cellulose, which is rich in hydroxyl (-OH) and other polar functional groups. The redistribution of electron density in the molecular orbital diagrams further supports this conclusion, as the adsorption of Safranin O onto cellulose results in significant delocalization of electron density over the cellulose surface, indicating strong host-guest interactions. In contrast, Acid-Blue 25, despite its relatively small energy gap, exhibits slightly weaker interactions with cellulose. This could be due to steric hindrance from its molecular structure, which may limit the extent of direct contact with the cellulose surface, reducing its adsorption efficiency. Furthermore, the polarity and solubility of Acid-Blue 25 in

aqueous solutions may influence its adsorption equilibrium, making it less likely to form strong bonds with cellulose compared to Safranin O. The observed differences in adsorption behavior are also evident in the molecular orbital distributions, where the electron density in the Cellulose@Safranin O complex shows broader delocalization, suggesting stronger electronic coupling between the dye and the adsorbent.

8.2. Characteristics of global reactivity

The quantum chemical parameters, including chemical hardness (η), softness (S), chemical potential (μ), electronegativity (χ), electrophilicity index (ω), and maximum charge transfer capacity (ΔNmax), provide valuable insights into the adsorption interactions between cellulose and the dye molecules Acid Blue 25 and Safranin O [103], as illustrated in Table 10. These parameters influence the electronic reactivity, charge transfer capabilities, and overall stability of the adsorbent-adsorbate complexes, thereby explaining the adsorption efficiency differences. Cellulose, as a pristine adsorbent, exhibits the highest chemical hardness (η = 3.19 eV) and the lowest softness (S = 0.31 eV), indicating its high stability and resistance to electronic perturbation. The high electronegativity (χ = 3.67 eV) suggests a moderate ability to attract electrons, while the high electrophilicity index (ω = 21.48 eV) implies that cellulose can act as a strong electron acceptor under favorable conditions. The total charge transfer capacity (ΔNmax = 1.15) is relatively low, reflecting its limited intrinsic ability to exchange electrons with other species. These properties suggest that while cellulose is chemically stable, its adsorption capacity relies heavily on external interactions such as hydrogen bonding and electrostatic attraction rather than direct charge transfer. The dyes, Acid-Blue 25 and Safranin O, exhibit significantly different electronic characteristics. Acid-Blue 25 has a lower chemical hardness (η = 1.11 eV) and higher softness (S = 0.90 eV), indicating that it is more chemically reactive and prone to electronic interactions. Its chemical potential (μ = −4.22 eV) and electronegativity (χ = 4.22 eV) are slightly higher than those of Safranin O, suggesting that it is a stronger electron acceptor. The electrophilicity index (ω = 9.88 eV) and charge transfer capacity (ΔNmax = 3.80) further confirm its moderate reactivity. On the other hand, Safranin O is even softer (S = 1.18 eV) and has a lower hardness (η = 0.85 eV), making it the most reactive species among the studied molecules. Its chemical potential (μ = −3.40 eV) and electronegativity (χ = 3.40 eV) suggest a slightly weaker electron-accepting ability compared to Acid-Blue 25, but its low electrophilicity index (ω = 4.91 eV) and high charge transfer capacity (ΔNmax = 4.00) indicate that it is more effective in electron donation, which can enhance interactions with cellulose through charge redistribution mechanisms. When cellulose interacts with these dyes to form the Cellulose@Acid-Blue 25 and Cellulose@Safranin O complexes, notable changes in electronic properties occur, reflecting their different adsorption behaviors. In the Cellulose@Acid-Blue 25 complex, the chemical hardness slightly increases to 1.17 eV, while the softness decreases to 0.86 eV, indicating a reduction in reactivity due to stabilization. The chemical potential shifts to −4.63 eV, suggesting an increased tendency to attract electrons, while the electronegativity rises to 4.63 eV. The electrophilicity index increases to 12.46 eV, indicating an enhancement in electron-accepting ability, and the charge transfer capacity (ΔNmax = 3.97) shows that significant electron exchange occurs between Acid-Blue 25 and cellulose. In contrast, the Cellulose@Safranin O complex exhibits a slightly higher chemical hardness (η = 1.35 eV) and lower softness (S = 0.74 eV), making it more stable than the Acid-Blue 25 complex. The chemical potential (−4.30 eV) and electronegativity (4.30 eV) indicate moderate electronic attraction, while the electrophilicity index (ω = 12.48 eV) remains nearly identical to that of the Cellulose@Acid-Blue 25 complex. However, the total charge transfer capacity (ΔNmax = 3.19) is lower than in the Acid-Blue 25 complex, suggesting that while Safranin O interacts strongly with cellulose, it relies more on electrostatic and π-π interactions rather than direct charge transfer. The observed trends support the experimental finding that cellulose adsorbs Safranin O more efficiently than Acid-Blue 25. Despite the slightly lower ΔNmax value for the Cellulose@Safranin O complex, the higher softness (S = 1.18 eV) and lower hardness (η = 0.85 eV) of free Safranin O suggest that it is highly reactive and can interact favorably with cellulose. Furthermore, its molecular structure, which contains aromatic rings and nitrogen-based functional groups, promotes strong π-π stacking and hydrogen bonding with cellulose. The enhanced stability of the Cellulose@Safranin O complex, along with its moderate charge transfer properties, explains why it has a greater affinity for cellulose than Acid-Blue 25. In contrast, Acid-Blue 25, despite its higher ΔNmax value in the complex, may experience steric hindrance and solubility-related effects that reduce its overall adsorption efficiency. The quantum descriptors confirm that Safranin O is a more suitable candidate for adsorption onto cellulose due to its higher softness, lower hardness, and strong electronic interactions. The Cellulose@Safranin O complex is more stable than the Cellulose@Acid-Blue 25 complex, which correlates with the observed higher adsorption efficiency of Safranin O onto cellulose.

8.3. MEP geometries

The Molecular Electrostatic Potential (MEP) maps provide crucial insights into the adsorption behavior of cellulose with Acid-Blue 25 and Safranin O by illustrating the charge distribution and potential interaction sites on the molecular surfaces. In these maps, regions of high electron density, often depicted in red, correspond to electrophilic sites, whereas areas of low electron density, shown in blue, represent nucleophilic sites. The MEP surface of cellulose (Fig. 14a) itself exhibits strong negative potential around oxygen-containing functional groups, particularly hydroxyl (-OH) groups, which serve as primary adsorption sites through hydrogen bonding and electrostatic interactions. When examining the MEP of the dye molecules, distinct differences emerge between Acid-Blue 25 and Safranin O, which explain their varying adsorption affinities toward cellulose. The MEP surface of Acid-Blue 25 (Fig. 14b) reveals a relatively uniform charge distribution with moderate electron-rich and electron-deficient regions, suggesting that it has limited strong electrostatic interaction potential with cellulose. On the other hand, Safranin O (Fig. 14c) exhibits highly localized regions of positive and negative electrostatic potential, particularly around nitrogen atoms and aromatic rings, which significantly enhance its interaction with cellulose's negatively charged oxygen sites. This pronounced charge separation in Safranin O leads to stronger electrostatic interactions, hydrogen bonding, and π-π stacking with cellulose, making it more favorably adsorbed compared to Acid-Blue 25. The post-adsorption MEP

Table 10
Global reactivity descriptors of cellulose, Acid-Blue 25, Safranin O, and their adsorbed complexes: Hardness (η), Softness (S), Chemical Potential (μ), Electronegativity (χ), Electrophilicity (ω), and Maximum Charge Transfer (ΔNmax).

Name of the molecules	η (hardness)	S (softness)	μ (chemical potential)	χ (electronegativity)	ω (electrophilicity)	ΔNmax (total charge transfer)
Cellulose	3.19	0.31	−3.67	3.67	21.48	1.15
Acid-Blue	1.11	0.90	−4.22	4.22	9.88	3.80
Safranin	0.85	1.18	−3.40	3.40	4.91	4.00
Cellulose@Acid-Blue 25	1.17	0.86	−4.63	4.63	12.46	3.97
Cellulose@Safranin O	1.35	0.74	−4.30	4.30	12.48	3.19

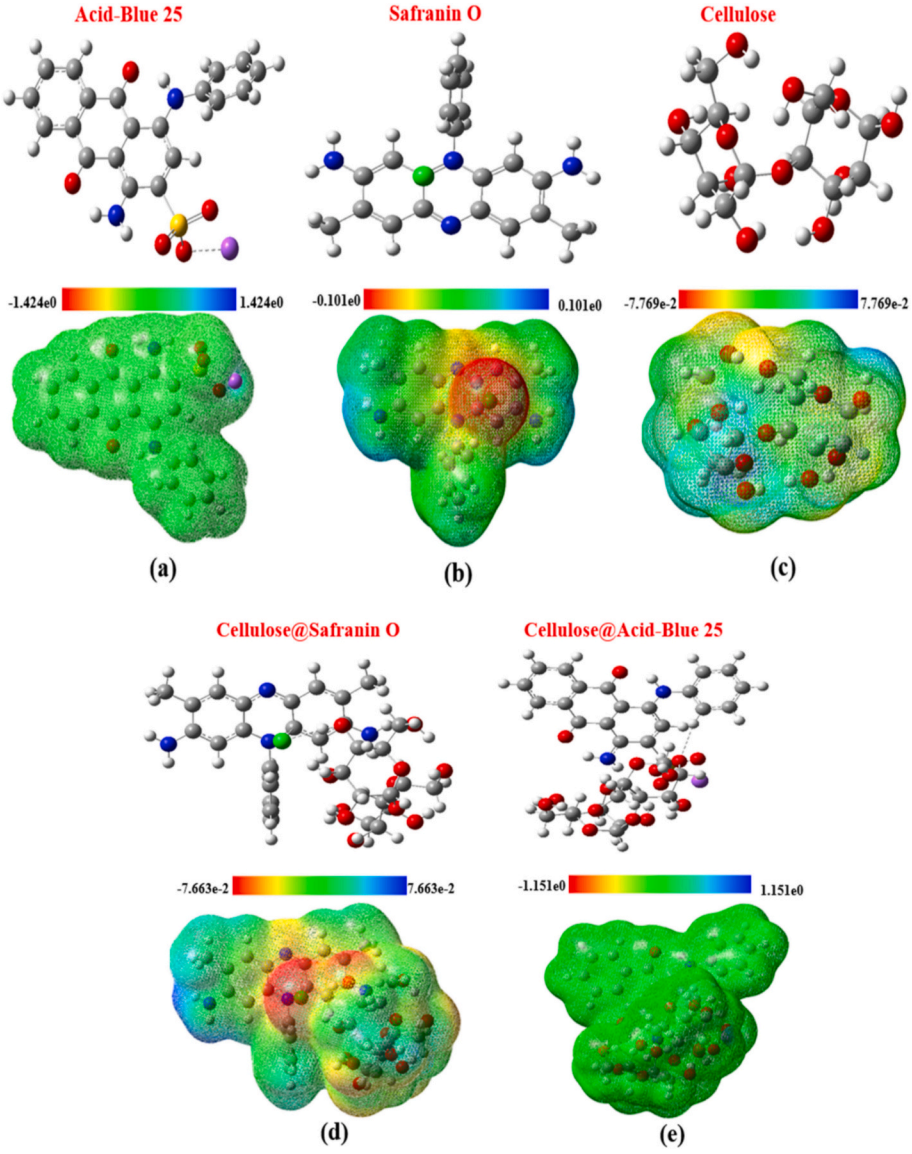

Fig. 14. Molecular structures and electrostatic potential maps of, (a) Acid-Blue 25, (b) Safranin O, (c) Cellulose, (d) Cellulose@Acid-Blue 25, (e) Cellulose@Safranin O, (f) Electrostatic Potential of Cellulose@Acid-Blue 25.

analysis further corroborates this observation, as evident in the charge redistribution on the cellulose@Safranin O and cellulose@Acid-Blue 25 complexes. The MEP surface of the cellulose@Safranin O (Fig. 14d) complex displays intense charge localization at the adsorption interface, indicating strong electrostatic interactions and hydrogen bonding between cellulose's hydroxyl groups and Safranin O's functional moieties, reinforcing its higher adsorption efficiency. In contrast, the MEP surface of the cellulose@Acid-Blue 25 (Fig. 14e) complex exhibits a more dispersed charge distribution, which suggests weaker electrostatic interactions and a lower affinity of cellulose for Acid-Blue 25, further supporting the experimental findings that cellulose adsorbs Safranin O more effectively than Acid-Blue 25.

8.4. Electrostatic interactions and adsorption behavior of Acid Blue 25 and Safranin O on cellulose: insights from Molecular Electrostatic Potential (MEP) maps under acidic and basic conditions

The Molecular Electrostatic Potential (MEP) maps under acidic and basic conditions provide crucial insights into the adsorption behavior of Acid Blue 25 and Safranin O on cellulose, as shown in Table 11. The MEP distribution highlights how charge distribution and electrostatic interactions influence the affinity of these dyes toward the cellulose surface, particularly in relation to the point of zero charge (pHzc) of cellulose at pH 4. Under acidic conditions, Acid Blue 25 exhibits a relatively uniform charge distribution with minimal highly polarized regions, as indicated by the predominantly green coloration [18]. This suggests that Acid Blue 25 has a lower tendency for strong electrostatic interactions under acidic conditions. However, since Acid Blue 25 achieves its highest adsorption between pH 3 and 4, this indicates that the dye likely interacts with cellulose through non-electrostatic interactions such as hydrogen bonding and van der Waals forces rather than strong Coulombic attraction. The MEP of Safranin O under acidic conditions is characterized by weak polarization, suggesting a limited electrostatic driving force for adsorption. This aligns with experimental observations that Safranin O does not adsorb efficiently in acidic environments due to its cationic nature, which experiences repulsion from the slightly positive cellulose surface below pH 4. Meanwhile, cellulose under acidic conditions displays a predominantly blue electrostatic potential, indicating a slightly electron-deficient surface, which may not strongly attract cationic species like Safranin O but could facilitate interactions

Table 11
Molecular Electrostatic Potential (MEP) maps of Acid Blue 25, Safranin O, and cellulose under acidic and basic conditions.

Acid Blue 25	Safranin O	Cellulose
Acid conditions		
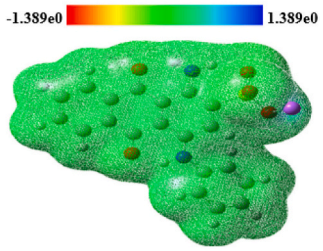	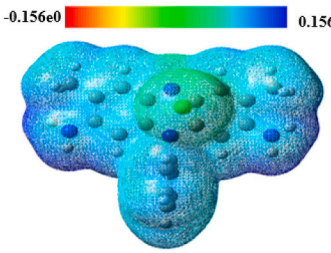	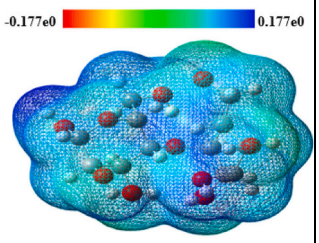
Basic conditions		
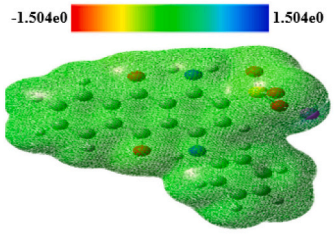	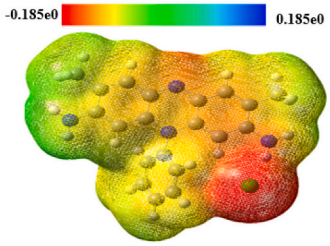	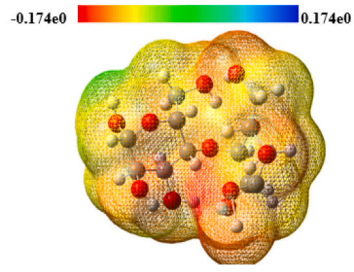

with anionic species. Under basic conditions, Acid Blue 25 exhibits a more intense green distribution, maintaining its weakly polarized structure, suggesting that it does not strongly interact with negatively charged cellulose in alkaline environments. This explains its lower adsorption above pH 4, as the increasing negative charge on the cellulose surface leads to repulsion between cellulose and Acid Blue 25. In contrast, Safranin O displays a highly polarized MEP with distinct red regions indicating strong electron density localization. This suggests an increased potential for electrostatic interactions, particularly with the negatively charged cellulose surface in basic conditions (pH $>$ 4). Since Safranin O exhibits its best adsorption between pH 6 and 9, this indicates that the strong electrostatic attraction between the negatively charged cellulose and the positively charged Safranin O plays a dominant role in its adsorption mechanism. The MEP map of cellulose in basic conditions shows a shift to more intense red and yellow regions, indicating an increase in negative surface charge, which enhances its affinity for cationic dyes like Safranin O while repelling anionic dyes such as Acid Blue 25. These demonstrate that adsorption efficiency is largely governed by the interplay between the charge of the adsorbate and the adsorbent. Since the pHzc of cellulose is 4, the surface is positively charged below this pH and negatively charged above it. This explains why Acid Blue 25, an anionic dye, is best adsorbed in slightly acidic conditions near pH 3–4, where the cellulose surface retains a positive charge. Conversely, Safranin O, a cationic dye, is best adsorbed in slightly basic conditions (pH 6–9), where the cellulose surface is negatively charged, promoting strong electrostatic attraction.

9. Adsorption mechanism of Acid Blue 25 and Safranin O onto cellulose

Fig. 15 presents a comprehensive illustration of the proposed adsorption mechanisms of Acid Blue 25 and Safranin O onto cactus-derived cellulose, highlighting the complex interplay of multiple physicochemical interactions responsible for dye retention. The cellulose framework, characterized by abundant hydroxyl, ether, and occasionally carboxyl functional groups, provides a highly reactive surface with numerous binding sites. These sites allow cellulose to interact with both anionic and cationic dyes through a combination of hydrogen bonding, electrostatic interactions, π–π stacking, and van der Waals forces, contributing to a stable and efficient adsorption process.

For Acid Blue 25, an anionic dye, adsorption is largely controlled by hydrogen bonding, electrostatic interactions, and π–π stacking. The hydroxyl groups of cellulose form hydrogen bonds with the amine and sulfonic groups of Acid Blue 25, providing strong, directional interactions that facilitate anchoring of dye molecules onto the cellulose surface. Electrostatic interactions also play a role: although the cellulose

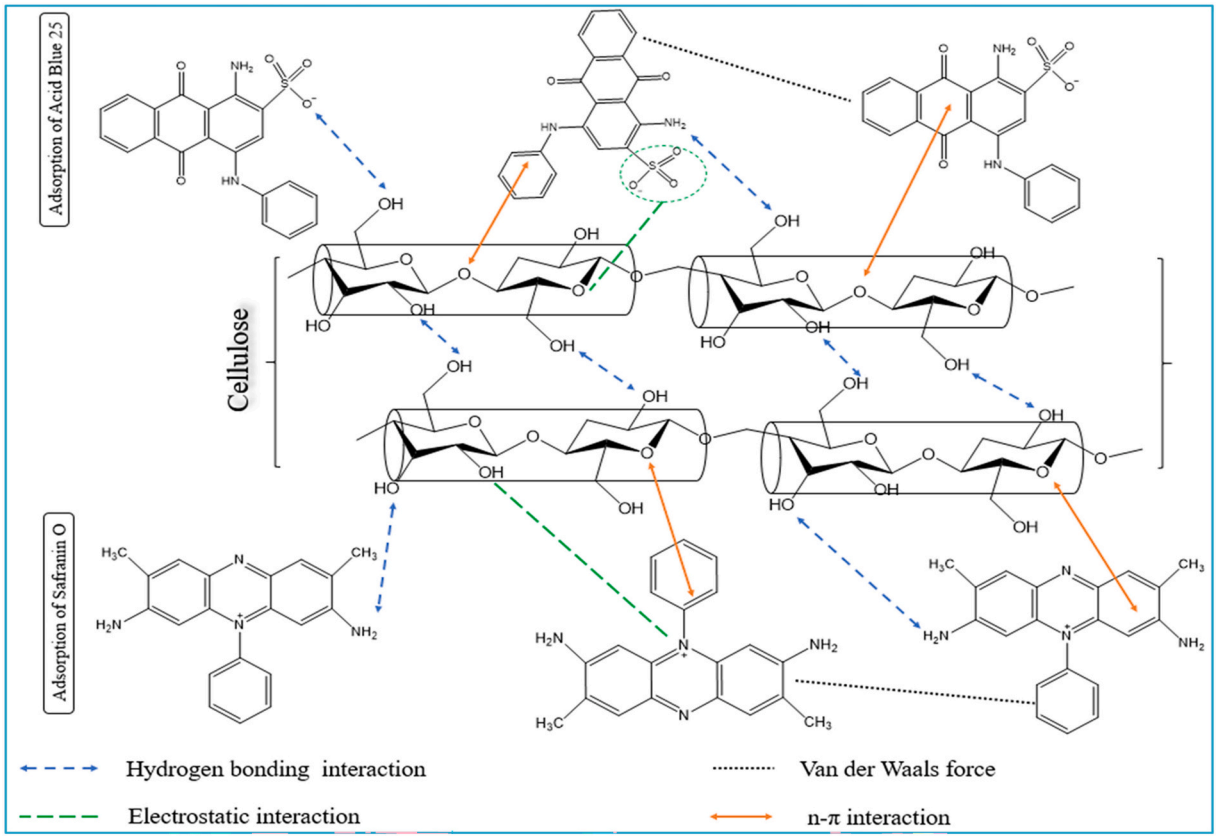

Fig. 15. Schematic representation of the interaction mechanisms involved in the adsorption of Acid Blue 25 and Safranin O onto cellulose.

surface is near neutral at pH 4 (close to its point of zero charge), partially positive sites on the cellulose interact with the negatively charged sulfonate groups of the dye, enhancing binding affinity. At higher pH values, where the cellulose surface becomes increasingly negative, adsorption decreases due to electrostatic repulsion between the negatively charged surface and the anionic dye. In addition, the aromatic rings of both Acid Blue 25 and cellulose can engage in π–π stacking interactions, further stabilizing the adsorption complex. Van der Waals forces also contribute to the retention of dye molecules, particularly at sites where specific interactions such as hydrogen bonding are limited, ensuring that even non-polar regions of the dye can be adsorbed. Collectively, these interactions result in moderate adsorption efficiency, which can be further influenced by solution parameters such as ionic strength and temperature.

In contrast, Safranin O, a cationic dye, exhibits adsorption predominantly governed by electrostatic attraction. The positively charged amino groups of Safranin O are strongly attracted to the negatively charged sites on the cellulose surface, particularly at pH values above the point of zero charge. This strong electrostatic interaction is the primary driver of adsorption and explains the higher removal efficiency of Safranin O compared to Acid Blue 25. Hydrogen bonding also contributes, with nitrogen-containing functional groups of the dye forming interactions with cellulose hydroxyl groups. Additionally, π–π interactions between the aromatic rings of Safranin O and cellulose further stabilize the adsorption complex. Van der Waals forces provide non-specific binding, ensuring that dye molecules adhere even in regions not directly involved in specific interactions. The combined effect of these forces produces a robust, multilayer adsorption process where dye molecules are tightly retained on the cellulose surface.

Moreover, the adsorption process is strongly influenced by the pKa values of the dyes and the pH of the solution, which together determine the ionization state of the dyes and the surface charge of the cellulose. Acid Blue 25 has a pKa of ~4.7, meaning it becomes predominantly deprotonated and negatively charged at pH values above this point, increasing repulsion with the negatively charged cellulose surface. Safranin O has a pKa of ~6.4, and at pH values above this, the dye remains cationic, favoring strong electrostatic attraction. This highlights that optimal adsorption occurs when electrostatic attraction is maximized and repulsion minimized, while hydrogen bonding and van der Waals interactions act as supportive mechanisms.

Additionally, competitive adsorption and site availability influence the mechanism. In real systems, multiple dye molecules may compete for the same active sites on the cellulose surface, which can reduce adsorption efficiency for one dye while favoring another, depending on charge and molecular size. Temperature and ionic strength can also modulate adsorption, as higher temperatures may disrupt weak

Table 12
Adsorption capacities of cellulose and other adsorbents.

	Adsorbents	q_{max} (mg/g)	References
Safranin O	Castor biomass	3.22	[104]
	Alginate/pomegranate peels beads	30.769	[105]
	Modified red mud	89.4	[4]
	MXene	33.95	[106]
	Guar gum succinate (GGS)	113.64	[5]
	κC-g-poly (AAC-co IA)/MWCNT	10.71	[107]
	Coconut coir–derived nanocellulose	79.3	[6]
	Cellulose	124.38	This work
Acid Blue 25	Baggase pith	17.5	[7]
	Peat	14.4	[108]
	Activated carbon from tobacco residue	0.96	[109]
	d polyethyleneimine functionalized tin (IV)-porphyrinic complex	14	[9]
	Activated carbon from *Citrus sinensis* leaf	543.47	[110]
	CuO-embedded chitosan	294.1	[111]
	Cellulose	11.07	This work

interactions such as van der Waals forces, and high ionic strength may screen electrostatic interactions, altering the binding dynamics.

In summary, the adsorption of Acid Blue 25 and Safranin O on cellulose is a multifaceted process involving synergistic effects of electrostatic attraction/repulsion, hydrogen bonding, π–π stacking, and van der Waals forces. Acid Blue 25 adsorption is limited by electrostatic repulsion at higher pH and relies more on hydrogen bonding and van der Waals forces, whereas Safranin O adsorption is strongly driven by electrostatic attraction and further stabilized by secondary interactions. This detailed mechanistic understanding underscores the versatility and efficiency of cellulose as a sustainable adsorbent capable of capturing both anionic and cationic dyes under varied environmental conditions, demonstrating its potential for practical wastewater treatment applications.

10. Comparison of adsorption capacities of cellulose with other adsorbents for the adsorption of Safranin O and Acid Blue 25 removal

Table 12 highlights the adsorption efficiencies (qmax) of various materials, providing insight into the potential of cellulose as a competitive adsorbent. The adsorption capacities of various adsorbents for Safranin O and Acid Blue 25 dyes reveal significant differences depending on their composition and surface characteristics. For Safranin O, the adsorption capacities ranged from 3.22 mg/g for castor biomass to 124.38 mg/g for the cellulose synthesized in this work. Traditional materials such as castor biomass and κC-*g*-poly(AAC-*co*-IA)/MWCNT exhibited relatively low adsorption performance, while modified materials like red mud (89.4 mg/g), MXene (33.95 mg/g), and coconut coir–derived nanocellulose (79.3 mg/g) demonstrated enhanced capacities due to increased surface area and functionalization. Notably, the cellulose prepared in this study showed the highest adsorption capacity (124.38 mg/g), indicating its superior efficiency toward Safranin O removal, likely attributed to its abundant hydroxyl groups, high porosity, and strong dye–surface interactions. In contrast, for Acid Blue 25, adsorption capacities varied widely among different adsorbents, ranging from 0.96 mg/g for activated carbon derived from tobacco residue to 543.47 mg/g for activated carbon obtained from *Citrus sinensis* leaves. Although some advanced composites such as CuO-embedded chitosan (294.1 mg/g) showed high adsorption potential, the cellulose synthesized in this work exhibited a moderate adsorption capacity of 11.07 mg/g. This result suggests that while the cellulose surface provides effective sites for cationic dye adsorption like Safranin O, its interaction with anionic dyes such as Acid Blue 25 is less favorable, possibly due to electrostatic repulsion between negatively charged dye molecules and the cellulose surface under experimental conditions.

11. Conclusion

This study successfully demonstrated the potential of cellulose extracted from cactus cladodes as an efficient, low-cost, and sustainable adsorbent for dye removal from aqueous solutions. The extraction process was optimized using Design-Expert software, achieving ideal conditions of 15 % NaOH, 98 °C, and 90 min, resulting in cellulose with enhanced surface area and active binding sites. The optimized material exhibited remarkable adsorption performance toward the cationic dye Safranin O, with a maximum capacity of 124.38 mg/g and a removal efficiency of 91.98 %, while the adsorption of the anionic dye Acid Blue 25 was less favorable (41.12 %), mainly due to electrostatic repulsion. Kinetic and isotherm analyses revealed that the adsorption followed a pseudo-second-order model and fitted well with the Langmuir isotherm, indicating chemisorption and monolayer adsorption on a homogeneous surface.

Thermodynamic results confirmed that the adsorption of Safranin O was spontaneous and exothermic, whereas that of Acid Blue 25 was non-spontaneous and endothermic. DFT simulations further supported these findings, showing stronger binding energies and charge-transfer interactions between Safranin O and cellulose. Collectively, these results highlight the effectiveness of cactus-derived cellulose as a renewable and eco-friendly adsorbent for cationic dye removal.

This work contributes to the advancement of green materials for wastewater treatment and demonstrates the value of integrating experimental optimization with theoretical modeling. Future research should focus on surface modification and composite formation to extend the adsorption capacity toward a broader spectrum of pollutants, reinforcing the role of cactus-derived cellulose in sustainable environmental remediation technologies.

CRediT authorship contribution statement

Soukaina El Bourachdi: Writing – original draft, Formal analysis, Data curation. **Abdelhay El Amri:** Software, Formal analysis, Data curation. **Ali Raza Ayub:** Software, Resources, Data curation, Conceptualization. **Yassine Rakcho:** Visualization, Supervision, Formal analysis, Data curation, Conceptualization. **Fatima Moussaoui:** Software, Formal analysis, Data curation. **Fatima Zahra Cherif:** Validation, Formal analysis. **Mahdi Lechheb:** Software, Formal analysis, Data curation. **Abdelali Grich:** Visualization, Software, Methodology. **Javier Araña:** Visualization, Validation, Supervision. **José Alberto Herrera-Melián:** Visualization, Validation, Supervision, Resources. **Amal Lahkimi:** Writing – review & editing, Visualization, Validation, Supervision.

Declaration of competing interest

The authors declare that they have no known competing financial interests or personal relationships that could have appeared to influence the work reported in this paper.

Data availability

Data will be made available on request.

References

[1] S. El Bourachdi, A. El Amri, A.R. Ayub, Y. Rakcho, F. Moussaoui, M. Lechheb, A. El-Bchiri, O.M. González Díaz, J.A. Herrera-Melián, A. Lahkimi, Green synthesis of high surface area of reduced graphene oxide via Aloe vera extract: characterization, DFT mechanistic insights, and enhanced Rhodamine B adsorption using Chitosan@EDTA@rGO composite, Surf. Interfaces 73 (2025), https://doi.org/10.1016/j.surfin.2025.107524.

[2] K. Loukili, S. Imame, M.K. El Bakkali, M. Lagseir, M. Sadoq, H. Atlas, S. El Bourachdi, A. Lahkimi, F. Boukhlifi, Application of Box-Behnken design for the optimization of crystal violet removal from aqueous solutions using acorn waste from Quercus ilex, E3S Web Conf. 649 (2025) 1–13, https://doi.org/10.1051/e3sconf/202564901019.

[3] S. Göktürk, M. Tunçay, Spectral studies of safranin-O in different surfactant solutions, Spectrochim. Acta - Part A Mol. Biomol. Spectrosc. 59 (2003) 1857–1866, https://doi.org/10.1016/S1386-1425(02)00418-3.

[4] M.K. Sahu, R.K. Patel, Removal of safranin-O dye from aqueous solution using modified red mud: kinetics and equilibrium studies, RSC Adv. 5 (2015) 78491–78501, https://doi.org/10.1039/c5ra15780c.

[5] J. Tripathi, S. Gupta, B.B. Mishra, Guar gum succinate: dry synthesis, characterization and application as an efficient adsorbent for removal of safranin-O dye, Carbohydr. Polym. 366 (2025) 123898, https://doi.org/10.1016/j.carbpol.2025.123898.

[6] V. Jakka, A. Goswami, A.K. Nallajarla, U. Roy, K. Srikanth, S. Sengupta, Coconut coir–derived nanocellulose as an efficient adsorbent for removal of cationic dye safranin-O: a detailed mechanistic adsorption study, Environ. Sci. Pollut. Res. 32 (2025) 19026–19047, https://doi.org/10.1007/s11356-023-29075-7.

[7] B. Chen, Chi Wai Hui, G. McKay, Film-pore diffusion modeling and contact time optimization for the adsorption of dyestuffs on pith, Chem. Eng. J. 84 (2001) 77–94, https://doi.org/10.1016/S1385-8947(01)00193-0.

[8] S. El, A. El, A. Raza, F. Moussaoui, Y. Rakcho, F. El, A. Adachi, T. Bouzid, A. Herrera-meli, Synthesis and characterization of avocado pit activated carbon-incorporated chitosan composite beads for harnessing methylene blue adsorption: DFT insights and box-behnken design optimization, J. Taiwan Inst. Chem. Eng. 173 (2025), https://doi.org/10.1016/j.jtice.2025.106142.

[9] R. Soury, M. Jabli, M. El Oudi, A. Haque, K.M. Alenezi, A. Al Otaibi, F. Abdulaziz, A. Bchetnia, Branched polyethyleneimine functionalized tin(IV)-porphyrinic complex: synthesis, characterization and application towards acid blue 25

adsorption from water, Results Chem. 13 (2025) 102022, https://doi.org/10.1016/j.rechem.2025.102022.
[10] A. Adachi, R. Soujoud, F. El Ouadrhiri, M. Tarik, A. Hmamou, N. Eloutassi, A. Lahkimi, Cactus and holm oak acorn for efficient textile wastewater treatment by coagulation-flocculation process optimization using Box-Benhken design, J. Ecol. Eng. 24 (2023) 315–328, https://doi.org/10.12911/22998993/162784.
[11] Y. Rakcho, M. Baidou, A. Naboulsi, A. Bouazizi, M. Mouiya, H. Sehaqui, Y. Abouliatim, A. Benhammou, M. Ouammou, A. Abourriche, J. Alami, Fabrication of low-cost ceramic nanofiltration membrane from natural resources for the removal of cationic and anionic dyes: experimental and DFT investigations, Chem. Eng. J. 505 (2025) 159779, https://doi.org/10.1016/j.cej.2025.159779.
[12] A. Adachi, F. El Ouadrhiri, E. Abdu Musad Saleh, F. Moussaoui, R.H. Althomali, S. El Bourachdi, K. Husain, A. Faris, I. Hassan, K. Azzaoui, B. Hammouti, A. Lahkimi, Enhancing hydrogen peroxide activation in heterogeneous Fenton reaction by codoping hydrochar with iron and copper, Arab. J. Chem. 17 (2024) 105862, https://doi.org/10.1016/J.ARABJC.2024.105862.
[13] S. El Bourachdi, A.R. Ayub, Y. Rakcho, A. El Amri, F. Moussaoui, F. El Ouadrhiri, A. Adachi, M. Jghaoui, T.E.H. Salmani, A. Lahkimi, Optimization of the degree of deacetylation of chitosan beads for efficient anionic dye adsorption: kinetics, thermodynamics, mechanistic insights via DFT analysis, and regeneration performance, Environ. Sci. Pollut. Res. 32 (2025) 7950–7975, https://doi.org/10.1007/s11356-025-36163-3.
[14] D.A. de R. Nogueira, T.M.P. Zanela, M.V. Machado, C.A.P. Almeida, R. Marangoni, Adsorption process of methyl orange dye onto zinc hydroxide nitrate: kinetic and thermodynamic studies, Colorants 2 (2023) 565–577, https://doi.org/10.3390/colorants2030028.
[15] B. Aurelien, T.T.D. Raoul, N.G. Ndifor-Angwafor, K.T. Arnaud, A.S. Gabche, Adsorption of 2,4-dinitrophenol on activated carbon prepared from cotton cakes: non-linear isotherm modeling, Chem. Sci. Int. J. 24 (2018) 1–20, https://doi.org/10.9734/csji/2018/43499.
[16] S.M. Qasim, Z.T. Al-Khateeb, F.A. Jabbar, M. Batool, L.S. Jasim, Adsorptive and reactivation potential of clay based superabsorbent kappa (κ)-carrageenan-graft-poly (acrylic acid-co-acrylamide)/ kaolin composite for malachite green dye: linear and non-linear modeling, J. Mol. Struct. 1348 (2025) 143448, https://doi.org/10.1016/j.molstruc.2025.143448.
[17] H.O. Jamel, M.H. Jasim, M.A. Mahdi, S.H. Ganduh, M. Batool, L.S. Jasim, M. N. Haider, Adsorption of Rhodamine B dye from solution using 3-((1-(4-((1H-benzo[d]imidazol-2-yl)amino)phenyl)ethylidene)amino)phenol (BIAPEHB)/P (AA-co-AM) composite, Desalin. Water Treat. 321 (2025) 101019, https://doi.org/10.1016/j.dwt.2025.101019.
[18] K. Benamar, S. El Bourachdi, A. Lahkimi, S. Ibnsouda, K. Fikri-benbrahim, Remediation of the cationic dye crystal violet using Olea oleaster leaf biomass, Int. J. Phytoremediation 0 (2025) 1–16, https://doi.org/10.1080/15226514.2025.2476092.
[19] G. Selvaraju, N.K.A. Bakar, Production of a new industrially viable green-activated carbon from Artocarpus integer fruit processing waste and evaluation of its chemical, morphological and adsorption properties, J. Clean. Prod. 141 (2017) 989–999, https://doi.org/10.1016/J.JCLEPRO.2016.09.056.
[20] A. Ramezani Kakroodi, S. Panthapulakkal, M. Sain, A. Asiri, Cellulose nanofibers from the skin of beavertail cactus, Opuntia basilaris, as reinforcements for polyvinyl alcohol, J. Appl. Polym. Sci. 132 (2015) 1–7, https://doi.org/10.1002/app.42499.
[21] Y.W. Abrha, H. Kye, J.W. Kang, Chemically treated cactus (Opuntia) as a sustainable biosorbent for the removal of heavy metals from aqueous solution: characterization and adsorption capacity, Desalin. Water Treat. 144 (2019) 345–354, https://doi.org/10.5004/dwt.2019.23580.
[22] X. Pang, L. Sellaoui, D. Franco, G.L. Dotto, J. Georgin, A. Bajahzar, H. Belmabrouk, A. Ben Lamine, A. Bonilla-Petriciolet, Z. Li, Adsorption of crystal violet on biomasses from pecan nutshell, para chestnut husk, araucaria bark and palm cactus: experimental study and theoretical modeling via monolayer and double layer statistical physics models, Chem. Eng. J. 378 (2019), https://doi.org/10.1016/j.cej.2019.122101.
[23] K. Benamar, S. El Bourachdi, A. Lahkimi, S. Ibnsouda, K. Fikri-benbrahim, Experimental study with RSM optimisation for methylene blue removal using an ecological approach blue removal using an ecological approach, Chem. Ecol. (2025) 1–24, https://doi.org/10.1080/02757540.2025.2474490.
[24] Y.W. Abrha, Y. Ahn, H. Kye, Y. Jung, Y. Yoon, T.M. Hwang, J.W. Kang, Adsorption of Pb2+ and Zn2+from aqueous solutions using dried powder of cactus opuntia: characterization, adsorption capacity and kinetics, Desalin. Water Treat. 135 (2018) 330–340, https://doi.org/10.5004/dwt.2018.22309.
[25] O. Tobbi, Z. Hattab, H. Boutefnouchet, B. Benouis, F. Benamia, R. Djellabi, Cost-effective walnut shell biosorbent for efficient Cr(VI) removal from water: batch adsorption and optimization using RSM-BBD, Desalin. Water Treat. 320 (2024) 100783, https://doi.org/10.1016/j.dwt.2024.100783.
[26] M. Lechheb, K. Essifi, S. El Bourachdi, H. Ouallal, M. El Ouali, B. Essafraoui, M. Azdouz, A. Lahkimi, M. Azrour, M. El Ouahabi, G. El Khadir, Optimisation of mechanical and thermal properties of clay bricks from Rissani-Morocco using Box-Behnken experimental design, Eur. J. Environ. Civ. Eng. 0 (2025) 1–21, https://doi.org/10.1080/19648189.2025.2458282.
[27] B.A. Geresu, M. Ebba, Investigations on the removal of phosphate and nitrate using a mixture of cactus and Moringa seed powder via RSM techniques, Desalin. Water Treat. 320 (2024) 100856, https://doi.org/10.1016/j.dwt.2024.100856.
[28] M. Contreras-Padilla, E.M. Rivera-Muñoz, E. Gutiérrez-Cortez, A.R. del López, M. E. Rodríguez-García, Characterization of crystalline structures in Opuntia ficus-indica, J. Biol. Phys. 41 (2015) 99–112, https://doi.org/10.1007/s10867-014-9368-6.
[29] N. Maslamani, S.B. Khan, E.M. Bakhsh, K. Akhtar, M. Alharbi, CuO-Fe2O3/calcium alginate-carboxymethylcellulose-chitosan as efficient nanocomposite beads for catalytic reduction of water pollutants, Results Chem. 13 (2025) 101936, https://doi.org/10.1016/j.rechem.2024.101936.
[30] A. Negrulescu, V. Patrulea, M. Mincea, C. Moraru, V. Ostafe, The adsorption of tartrazine, congo red and methyl orange on chitosan beads, Dig. J. Nanomater. Biostruct. 9 (2014) 45–52.
[31] S. El Bourachdi, A. El Amri, A.R. Ayub, F. Moussaoui, Y. Rakcho, F. El Ouadrhiri, A. Adachi, M. Lechheb, J.A. Herrera-Melián, A. Lahkimi, Development of a novel low-cost adsorbent Chitosan@EDTA@Cellulose composite to effectively remove Methyl Orange dye from wastewater: experimental and theoretical investigation, Int. J. Biol. Macromol. 305 (2025), https://doi.org/10.1016/j.ijbiomac.2025.141030.
[32] E.W.E.S. Shahrin, N.A.H. Narudin, N.N.M. Shahri, S.B. Verinda, M. Nur, J. Hobley, A. Usman, Adsorption behavior and dynamic interactions of anionic acid blue 25 on agricultural waste, Molecules 27 (2022) 1–13, https://doi.org/10.3390/molecules27051718.
[33] A. Benhamou, A. Boussetta, N. Grimi, M. El Idrissi, M. Nadifiyine, F.J. Barba, A. Moubarik, Characteristics of cellulose fibers from Opuntia ficus indica cladodes and its use as reinforcement for PET based composites, J. Nat. Fibers 19 (2022) 6148–6164, https://doi.org/10.1080/15440478.2021.1904484.
[34] F. Prieto-García, E. Jiménez-Muñoz, O.A. Acevedo-Sandoval, R. Rodríguez-Laguna, R.A. Canales-Flores, J. Prieto-Méndez, Obtaining and optimization of cellulose pulp from leaves of Agave tequilana Weber Var. Blue. Preparation of handmade craft paper, Waste Biomass Valoriz. 0 (2019) 2379–2395, https://doi.org/10.1007/s12649-018-0262-5.
[35] N.E. Fitriana, A. Suwanto, T.H. Jatmiko, S. Mursiti, D.J. Prasetyo, Cellulose extraction from sugar palm (Arenga pinnata) fibre by alkaline and peroxide treatments, IOP Conf. Ser. Earth Environ. Sci. 462 (2020), https://doi.org/10.1088/1755-1315/462/1/012053.
[36] C. Le, D.C. Stuckey, Colorimetric measurement of carbohydrates in biological wastewater treatment systems: a critical evaluation, Water Res. 94 (2016) 280–287, https://doi.org/10.1016/j.watres.2016.03.008.
[37] M.A. Lukáš Kejla, Tim Schulzke, Pavel Šimáček, Anthrone method combined with adsorption of interferents as a new approach towards reliable quantification of total carbohydrate content in pyrolysis bio-oils ˇa Luk a, J. Anal. Appl. Pyrolysis 173 (2023), https://doi.org/10.1016/j.jaap.2023.106066.
[38] F. El Ouadrhiri, E. Abdu Musad Saleh, K. Husain, A. Adachi, A. Hmamou, I. Hassan, M. Mostafa Moharam, A. Lahkimi, Acid assisted-hydrothermal carbonization of solid waste from essential oils industry: optimization using I-optimal experimental design and removal dye application, Arab. J. Chem. 16 (2023), https://doi.org/10.1016/j.arabjc.2023.104872.
[39] F. El Ouadrhiri, R.H. Althomali, A. Adachi, E. Abdu Musad Saleh, K. Husain, A. Lhassani, I. Hassan, M. Mostafa Moharam, A.F. Kassem, M. Chaouch, M. Ali Oturan, A. Lahkimi, Nitrogen and phosphorus co-doped carbocatalyst for efficient organic pollutant removal through persulfate-based advanced oxidation processes, J. Saudi Chem. Soc. 27 (2023), https://doi.org/10.1016/j.jscs.2023.101648.
[40] H.S. AlSalem, R.A.S. Alatawi, A.A.H. Bukhari, J.S. Alnawmasi, I. Zghab, M.G. El-Desouky, M.H. Almabadi, Z.H. Alnakhli, N.H. Elsayed, Adsorption and removal of Pb (II) via layer double hydroxide encapsulated with chitosan; synthesis, characterization adsorption isotherms, kinetics, thermodynamics, & optimization via Box-Behnken design, Int. J. Biol. Macromol. 283 (2024), https://doi.org/10.1016/j.ijbiomac.2024.137517.
[41] S. El, F. Moussaoui, A. El, F. El, A. Adachi, A. Bendaoud, A. Mounadi, DFT theoretical analysis, experimental approach, and RSM process to understand the congo red adsorption mechanism on Chitosan@Graphene oxide beads, J. Mol. Struct. 1321 (2025) 140090, https://doi.org/10.1016/j.molstruc.2024.140090.
[42] L. Khezami, N. Elamin, A. Modwi, K.K. Taha, M.S. Amer, M. Bououdina, Mesoporous Sn@TiO2 nanostructures as excellent adsorbent for Ba ions in aqueous solution, Ceram. Int. 48 (2022) 5805–5813, https://doi.org/10.1016/J.CERAMINT.2021.11.128.
[43] H. Yazid, T. Bouzid, M. El Himri, A. Regti, M. El Haddad, Bisphenol A (BPA) remediation using walnut shell as activated carbon employing experimental design for parameter optimization and theoretical study to establish the adsorption mechanism, Inorg. Chem. Commun. 161 (2024), https://doi.org/10.1016/j.inoche.2024.112064.
[44] A. Dabagh, R. Benhiti, M. EL-Habacha, A. Ait Ichou, M. Abali, A. Assouani, M. Guellaa, A. Berisha, R. Hsissou, F. Sinan, M. Zerbet, Application of Taguchi method, response surface methodology, DFT calculation and molecular dynamics simulation into the removal of orange G and crystal violet by treated biomass, HDabagh, A., Benhiti, R., EL-Habacha, M., Ait Ichou, A., Abali, M., Assouani, A., Guellaa, M., Berisha, A., Hsissou, R., Sinan, F., Zerbet, M., 2023, in: Appl. Taguchi Method, Response Surf. Methodol. DFT Calc. Mol. Dyn. Simul 9, 2023, p. e21977, https://doi.org/10.1016/j.heliyon.2023.e21977.
[45] Sumanjit, S. Rani, R.K. Mahajan, Equilibrium, kinetics and thermodynamic parameters for adsorptive removal of dye Basic Blue 9 by ground nut shells and Eichhornia, Arab. J. Chem. 9 (2016) S1464–S1477, https://doi.org/10.1016/j.arabjc.2012.03.013.
[46] E.D. Revellame, D.L. Fortela, W. Sharp, R. Hernandez, M.E. Zappi, Adsorption kinetic modeling using pseudo-first order and pseudo-second order rate laws: a review, Clean. Eng. Technol. 1 (2020) 100032, https://doi.org/10.1016/j.clet.2020.100032.

[47] K. Mabalane, N.D. Shooto, P.M. Thabede, A novel permanganate and peroxide carbon-based avocado seed waste for the adsorption of manganese and chromium ions from water, Case Stud. Chem. Environ. Eng. 10 (2024) 100782, https://doi.org/10.1016/j.cscee.2024.100782.
[48] J. Chen, F. Ma, Y. Qin, J. Li, P. Yang, Preparation and characterization of sodium lignosulfonate-chitosan hydrochloride composite materials for dye adsorption, React. Funct. Polym. 208 (2025) 106150, https://doi.org/10.1016/j.reactfunctpolym.2025.106150.
[49] A. Yildirim, H. Acay, Methylene blue and malachite green dyes adsorption onto russula delica/bentonite/tripolyphosphate, Heliyon 11 (2025) e41250, https://doi.org/10.1016/j.heliyon.2024.e41250.
[50] K. Kriti, G.S. Kumar, S. Chauhan, S. Chauhan, Sharma, Epichlorohydrin/triethylamine modified psyllium as a highly efficient adsorbent for selective adsorption of anionic dyes, Int. J. Biol. Macromol. 294 (2025) 139386, https://doi.org/10.1016/j.ijbiomac.2024.139386.
[51] H. Mo, L. Liu, Z. Yang, Y. Lao, Y. He, The effect of magnesium oxide on the structure of metakaolin-based geopolymer microspheres and its application in the adsorption of methylene blue dye, J. Water Process Eng. 70 (2025) 106937, https://doi.org/10.1016/j.jwpe.2025.106937.
[52] D. A.O, Langmuir, Freundlich, Temkin and Dubinin–Radushkevich isotherms studies of equilibrium sorption of Zn 2+ unto phosphoric acid modified rice husk, IOSR J. Appl. Chem. 3 (2012) 38–45, https://doi.org/10.9790/5736-0313845.
[53] N.K. Mondal, A. Samanta, S. Dutta, S. Chattoraj, Optimization of Cr(VI) biosorption onto Aspergillus niger using 3-level Box-Behnken design: equilibrium, kinetic, thermodynamic and regeneration studies, J. Genet. Eng. Biotechnol. 15 (2017) 151–160, https://doi.org/10.1016/j.jgeb.2017.01.006.
[54] M. Khnifira, W. Boumya, J. Atarki, M. Sadiq, M. Achak, A. Bouich, N. Barka, M. Abdennouri, Experimental, DFT and MD simulation combined studies for the competitive adsorption of anionic and cationic dyes on activated carbon in an aqueous medium, J. Mol. Struct. 1310 (2024) 138247, https://doi.org/10.1016/j.molstruc.2024.138247.
[55] C.M.D. Carvalho, F.O. Sanches-Neto, V.H. Carvalho-Silva, D.P.R. Ascheri, R. Signini, Response surface and DFT protocols for improvement of the adsorption process of lignocellulosic-based biomass for the removal of basic dyes, Int. J. Biol. Macromol. 275 (2024), https://doi.org/10.1016/j.ijbiomac.2024.133208.
[56] A.A. El Hassani, K. Tanji, I. El Mrabet, Y. Fahoul, A. El Gaidoumi, A.T. Benjelloun, M. Sfaira, H. Zaitan, A. Kherbeche, A combined molecular dynamics simulation, DFT calculations, and experimental study of the adsorption of Rhodamine B dye on kaolinite and hydroxyapatite in aqueous solutions, Surf. Interfaces 36 (2023) 102647, https://doi.org/10.1016/j.surfin.2023.102647.
[57] Y. Achour, L. Bahsis, E.H. Ablouh, H. Yazid, M.R. Laamari, M. El Haddad, Insight into adsorption mechanism of Congo red dye onto Bombax Buonopozense bark activated-carbon using central composite design and DFT studies, Surf. Interfaces 23 (2021) 100977, https://doi.org/10.1016/j.surfin.2021.100977.
[58] H. Luo, X. Huang, Y. Luo, Z. Li, L. Li, C. Gao, J. Xiong, W. Li, Adsorption behavior and mechanism of acidic blue 25 dye onto cucurbit[8]uril: a spectral and DFT study, Spectrochim. Acta - Part A Mol. Biomol. Spectrosc. 193 (2018) 125–132, https://doi.org/10.1016/j.saa.2017.12.006.
[59] H. He, F. An, Y. Wang, W. Wu, Z. Huang, H. Song, Effects of pretreatment, NaOH concentration, and extraction temperature on the cellulose from Lophatherum gracile Brongn, Int. J. Biol. Macromol. 190 (2021) 810–818, https://doi.org/10.1016/j.ijbiomac.2021.09.041.
[60] A.A. Modenbach, Effects of sodium hydroxide pretreatment on structural components of biomass, Trans. ASABE (2014) 1187–1198, https://doi.org/10.13031/trans.57.10046.
[61] V.J. Inglezakis, S.G. Poulopoulos, H. Kazemian, Insights into the S-shaped sorption isotherms and their dimensionless forms, Microporous Mesoporous Mater. 272 (2018) 166–176, https://doi.org/10.1016/j.micromeso.2018.06.026.
[62] S. Wang, O. Salim, M. Piri, The effects of pore shape and geometry on the storage of CO2 in mesoporous media, Mater. Today Sustain. 29 (2025), https://doi.org/10.1016/j.mtsust.2025.101076.
[63] F. Elayadi, W. Boumya, M. Achak, Y. Chhiti, F.E.M.hamd. Alaoui, N. Barka, C. El Adlouni, Experimental and modeling studies of the removal of phenolic compounds from olive mill wastewater by adsorption on sugarcane bagasse, Environ. Chall. 4 (2021), https://doi.org/10.1016/j.envc.2021.100184.
[64] F.O. Afolabi, P. Musonge, B.F. Bakare, Application of the response surface methodology in the removal of Cu2+ and Pb2+ from aqueous solutions using orange peels, Sci. Afr. 13 (2021) e00931, https://doi.org/10.1016/j.sciaf.2021.e00931.
[65] P.S. Ardekani, H. Karimi, M. Ghaedi, A. Asfaram, M.K. Purkait, Ultrasonic assisted removal of methylene blue on ultrasonically synthesized zinc hydroxide nanoparticles on activated carbon prepared from wood of cherry tree: experimental design methodology and artificial neural network, J. Mol. Liq. 229 (2017) 114–124, https://doi.org/10.1016/j.molliq.2016.12.028.
[66] N. Genç, Ö. Kılıçoğlu, A.O. Narci, Removal of Bisphenol A aqueous solution using surfactant-modified natural zeolite: Taguchi's experimental design, adsorption kinetic, equilibrium and thermodynamic study, Environ. Technol. (UK) 38 (2017) 424–432, https://doi.org/10.1080/21622515.2016.1196739.
[67] S. Ai, K. Gao, W. Yu, L. Liu, Fabrication of cellulose-based carboxylate-functionalized materials via cosolubilization-crystallization for reversible Pb2+ adsorption, Environ. Technol. Innov. 37 (2025) 104058, https://doi.org/10.1016/j.eti.2025.104058.
[68] T. Sherwyn, N. Nadia, N. Najhan, D. Trache, M.H. Hussin, Kinetics and equilibrium studies of congo red adsorption using alginate hydrogel beads impregnated with coconut shell derived-cellulose nanocrystals, J. Ind. Eng. Chem. (2025), https://doi.org/10.1016/j.jiec.2025.02.024.
[69] Y. Kim, D. Jeong, K.H. Park, J.H. Yu, S. Jung, Efficient adsorption on benzoyl and stearoyl cellulose to remove phenanthrene and pyrene from aqueous solution, Polymers (Basel) 10 (2018), https://doi.org/10.3390/POLYM10091042.
[70] S. Cheng, A. Huang, S. Wang, Q. Zhang, Effect of different heat treatment temperatures on the chemical composition and structure of Chinese fir wood, BioResources 11 (2016) 4006–4016, https://doi.org/10.15376/biores.11.2.4006-4016.
[71] B. Abderrahim, E. Abderrahman, A. Mohamed, T. Fatima, T. Abdesselam, O. Krim, Kinetic thermal degradation of cellulose, polybutylene succinate and a green composite: comparative study, world, J. Environ. Eng. 3 (2015) 95–110, https://doi.org/10.12691/WJEE-3-4-1. Vol. 3, 2015, Pages 95-110.
[72] M. El-sakhawy, S. Kamel, A. Salama, H. Sarhan, Preparation and infrared study of cellulose based amphiphilic materials, Cellulose Chem. Technol. 52 (3–4) (2018) 193–200.
[73] E.M.S. Hassani, I. Mehdaoui, D. Azzouni, R. Mahmoud, A. Taleb, G.F. Wondmie, A.M. Salamatullah, M. Bourhia, S. Ibenmoussa, M. Taleb, Z. Rais, Elaboration of an innovative plant biomaterial for its valorization in the treatment of wastewater, Bioresour. Bioprocess. 11 (2024), https://doi.org/10.1186/s40643-024-00774-4.
[74] A.K. Siddhanta, M.U. Chhatbar, G.K. Mehta, N.D. Sanandiya, S. Kumar, M.D. Oza, K. Prasad, R. Meena, The cellulose contents of Indian seaweeds, J. Appl. Phycol. 23 (2011) 919–923, https://doi.org/10.1007/s10811-010-9599-2.
[75] C. Orrabalis, D. Rodríguez, L.G. Pampillo, C. Londoño-Calderón, M. Trinidad, R. Martínez-García, Characterization of nanocellulose obtained from Cereus forbesii (a South American cactus), Mater. Res. 22 (2019) 1–10, https://doi.org/10.1590/1980-5373-MR-2019-0243.
[76] S.K. Jang, H. Jeong, I.G. Choi, The effect of cellulose crystalline structure modification on glucose production from chemical-composition-controlled biomass, Sustainability 15 (2023) 1–12, https://doi.org/10.3390/su15075869.
[77] Y. Nishiyama, J. Sugiyama, H. Chanzy, P. Langan, Crystal structure and hydrogen bonding system in cellulose Iα from synchrotron X-ray and neutron fiber diffraction, J. Am. Chem. Soc. 125 (2003) 14300–14306, https://doi.org/10.1021/ja037055w.
[78] R.M. Silva, V.X.M. de Carvalho, V.C. Dumont, M.H. Santos, A.M.M.L. Carvalho, Addition of mechanically processed cellulosic fibers to ionomer cement: mechanical properties, Braz. Oral Res. 29 (2015) 1–8, https://doi.org/10.1590/1807-3107BOR-2015.vol29.0030.
[79] J. Lozano-montante, R. Garza-hern, S. Mario, E. Moran-palacio, G. Niño-medina, M. Almada, L. Hern, Cellulose to adsorb Pb (II) from water, Polymers (Basel) 13 (2021) 3166.
[80] N. Kumar, B. Kumar, H. Gupta, A. Kumar, Development and evaluation of cellulose/graphene-oxide based composite for removing phenol from aqueous solutions, Polymers (Basel) 15 (2023) 1–16, https://doi.org/10.3390/polym15030572.
[81] B. Abbar, A. Alem, S. Marcotte, A. Pantet, N.D. Ahfir, L. Bizet, D. Duriatti, Experimental investigation on removal of heavy metals (Cu2+, Pb2+, and Zn2+) from aqueous solution by flax fibres, Process Saf. Environ. Prot. 109 (2017) 639–647, https://doi.org/10.1016/j.psep.2017.05.012.
[82] J. Mittal, R. Ahmad, A. Mittal, Kahwa tea (Camellia sinensis) carbon — a novel and green low-cost adsorbent for the sequestration of titan yellow dye from its aqueous solutions, Desalin. Water Treat. 227 (2021) 404–411, https://doi.org/10.5004/dwt.2021.27284.
[83] M. Asheghmoalla, M. Mehrvar, Adsorption of a multicomponent pharmaceutical wastewater on charcoal-based activated carbon: equilibrium and kinetics, Water (Switzerland) 16 (2024), https://doi.org/10.3390/w16152086.
[84] F. Sharifipour, S. Hojati, A. Landi, Kinetics and thermodynamics of lead adsorption from aqueous solutions onto Iranian sepiolite and zeolite characterization of Iranian sepiolite: physical and environmental applications view project, Artic, Int. J. Environ. Res. 9 (2015) 1001–1010. Summer.
[85] A. Ebrahimian Pirbazari, E. Saberikhah, M. Badrouh, M.S. Emami, Alkali treated Foumanat tea waste as an efficient adsorbent for methylene blue adsorption from aqueous solution, Water Resour. Ind. 6 (2014) 64–80, https://doi.org/10.1016/j.wri.2014.07.003.
[86] V. Patrulea, A. Negrulescu, S. Writing, L. Pitulice, Optimization of the Removal of Copper(II) Ions From Aqueous Solution on Chitosan and Cross-linked Chitosan Beads, 2013, https://doi.org/10.15376/biores.8.1.1147-1165.
[87] T.S. Alomar, M.A. Habila, N. Almasoud, Z.A. Alothman, M. Sheikh, M. Soylak, Biomass - Derived Adsorbent for Dispersive Solid - Phase Extraction of Cr (III), Fe (III), Co (II) and Ni (II) From Food Samples Prior to ICP - MS Detection, 2021.
[88] N.L. Ahmad, U.Z. Zakariyya, N.G. Zaharaddeen, et al., Rice husk as biosorbent for the adsorption of methylene blue, Sci. World J. 14 (2019) 66–70.
[89] A. Adachi, F. El Ouadrhiri, I. El Manssouri, F. Moussaoui, S. El Bourachdi, A. Lahkimi, Removal of dyes by adsorption process using date pits as material environmentally friendly, Ecol. Eng. Environ. Technol. 24 (2023) 181–193, https://doi.org/10.12912/27197050/171494.
[90] I. Lebkiri, B. Abbou, L. Kadiri, A. Ouass, A. Elamri, H. Ouaddari, O. Elkhattabi, A. Lebkiri, E.H. Rifi, Swelling properties and basic dye adsorption studies of polyacrylamide hydrogel, Desalin. Water Treat. 233 (2021) 361–376, https://doi.org/10.5004/dwt.2021.27530.
[91] A.E.L. Amri, J. Bensalah, Y. Essaadaoui, I. Lebkiri, B. Abbou, A. Zarrouk, E.H. Rifi, A. Lebkiri, Elaboration, characterization and performance evaluation of a new environmentally friendly adsorbent material based on the reed filter (Typha Latifolia): kinetic and thermodynamic studies and application in the adsorption of Cd (II) ion, Chem. Data Collect. 39 (2022) 100849, https://doi.org/10.1016/j.cdc.2022.100849.

[92] J. Bensalah, H. Ouaddari, Ş. Erdoğan, B. Tüzün, A.R.Z. Gaafar, H.A. Nafidi, M. Bourhia, A. Habsaoui, Cationic resin polymer A®IRC-50 as an effective adsorbent for the removal of Cr(III), Cu(II), and Ag(I) from aqueous solutions: a kinetic, mathematical, thermodynamic and modeling study, Inorg. Chem. Commun. 157 (2023), https://doi.org/10.1016/j.inoche.2023.111272.
[93] A. El Amri, J. Bensalah, A. Idrissi, K. Lamya, A. Ouass, S. Bouzakraoui, A. Zarrouk, E.H. Rifi, A. Lebkiri, Adsorption of a cationic dye (methylene bleu) by Typha latifolia: equilibrium, kinetic, thermodynamic and DFT calculations, Chem. Data Collect. 38 (2022) 100834, https://doi.org/10.1016/j.cdc.2022.100834.
[94] M. Elabboudi, J. Bensalah, A. El Amri, N. EL Azzouzi, B. Srhir, A. Lebkiri, A. Zarrouk, E.H. Rifi, Adsorption performance and mechanism of anionic MO dye by the adsorbent polymeric Amberlite®IRA-410 resin from environment wastewater: equilibrium kinetic and thermodynamic studies, J. Mol. Struct. 1277 (2023), https://doi.org/10.1016/j.molstruc.2022.134789.
[95] Y. Miyah, M. Benjelloun, F. Mejbar, S. Ssouni, M. El-Habacha, S. Iaich, N. El Messaoudi, M. Zerrouq, M. Souilah, A. Lahrichi, F. Zerrouq, CWPO mechanism for toxic dye degradation in the presence of Cu@FbHAp catalyst: DFT study, performance analysis, response surface methodology, regeneration, and cost estimation, Results Chem. 13 (2025) 102038, https://doi.org/10.1016/j.rechem.2025.102038.
[96] A. Dabagh, M. EL-Habacha, A. Assouani, G. Mahmoudy, A.A. Ichou, R. Benhiti, F. Sinan, M. Zerbet, Remediation of hazardous dyes on low-cost biosorbent: batch and dynamic adsorption, phytotoxicity assessment, and application of industrial wastewater, Biomass Convers. Biorefinery (2025), https://doi.org/10.1007/s13399-025-06531-7.
[97] S. Lagdali, M. El-Habacha, G. Mahmoudy, M. Benjelloun, S. Ssouni, Y. Miyah, S. Iaich, M. Zerbet, Development and characterization of an asymmetrical flat microfiltration membrane based on natural phengite clay: application as a pretreatment for raw seawater reverse osmosis desalination, J. Water Process Eng. 67 (2024) 106253, https://doi.org/10.1016/j.jwpe.2024.106253.
[98] S. Lagdali, Y. Miyah, M. El-Habacha, G. Mahmoudy, M. Benjelloun, S. Iaich, M. Zerbet, M. Chiban, F. Sinan, Performance assessment of a phengite clay-based flat membrane for microfiltration of real-wastewater from clothes washing: characterization, cost estimation, and regeneration, Case Stud. Chem. Environ. Eng. 8 (2023) 100388, https://doi.org/10.1016/j.cscee.2023.100388.
[99] H. Duarte, J. Brás, E.M.S. Hassani, M.J. Aliaño-Gonzalez, S. Magalhães, L. Alves, A.J.M. Valente, A. Eivazi, M. Norgren, A. Romano, B. Medronho, Lignin-furanic rigid foams: enhanced methylene blue removal capacity, recyclability, and flame retardancy, Polymers (Basel) 16 (2024), https://doi.org/10.3390/polym16233315.
[100] E.M. Saoudi Hassani, H. Duarte, J. Brás, A. Taleb, M. Taleb, Z. Rais, A. Eivazi, M. Norgren, A. Romano, B. Medronho, On the valorization of olive oil pomace: a sustainable approach for methylene blue removal from aqueous media, Polymers (Basel) 16 (2024), https://doi.org/10.3390/polym16213055.
[101] T. Delgado-Montiel, R. Soto-Rojo, J. Baldenebro-López, D. Glossman-Mitnik, Theoretical study of the effect of different π bridges including an azomethine group in triphenylamine-based dye for dye-sensitized solar cells, Molecules 24 (2019) 1–16, https://doi.org/10.3390/molecules24213897.
[102] A. Escobedo-Morales, L. Tepech-Carrillo, A. Bautista-Hernández, J.H. Camacho-García, D. Cortes-Arriagada, E. Chigo-Anota, Effect of chemical order in the structural stability and physicochemical properties of B12N12 fullerenes, Sci. Rep. 9 (2019) 1–12, https://doi.org/10.1038/s41598-019-52981-1.
[103] U. Rehman, A. Mansha, M. Zahid, S. Asim, A.F. Zahoor, Z.A. Rehan, Quantum mechanical modeling unveils the effect of substitutions on the activation barriers of the Diels–Alder reactions of an antiviral compound 7H-benzo[a]phenalene, Struct. Chem. 33 (2022) 1907–1920, https://doi.org/10.1007/s11224-022-01948-6.
[104] M. Suleman, M. Zafar, A. Ahmed, M.U. Rashid, S. Hussain, A. Razzaq, N. A. Mohidem, T. Fazal, B. Haider, Y.K. Park, Castor leaves-based biochar for adsorption of safranin from textile wastewater, Sustainability 13 (2021), https://doi.org/10.3390/su13126926.
[105] A. Abbaz, S. Arris, G. Viscusi, A. Ayat, H. Aissaoui, Y. Boumezough, Adsorption of safranin O dye by alginate/pomegranate peels beads: kinetic, isotherm and thermodynamic studies, Gels 9 (2023), https://doi.org/10.3390/gels9110916.
[106] S. Sarkar, S. Mukherjee, A. Saha, A. Bhowal, P. Das, Functionalized MXene nanosheets for efficient safranin dye removal from aqueous solution: a batch study and RSM optimized parameters, Surf. Interfaces 68 (2025) 106636, https://doi.org/10.1016/j.surfin.2025.106636.
[107] N.A. Hussain, L.S. Jasim, Synthesis and characterization of kappa (κ)-carrageenan-grafted poly (acrylic acid-co-itaconic acid)/ multi-walled carbon nanotube (κC-g-poly (AAC-co-IA)/ MWCNT) composite for removing safranin-o dye from aqueous solution, Process Saf. Environ. Prot. 195 (2025) 106828, https://doi.org/10.1016/j.psep.2025.106828.
[108] Y.S. Ho, G. McKay, Sorption of dyes and copper ions onto biosorbents, Process Biochem. 38 (2003) 1047–1061, https://doi.org/10.1016/S0032-9592(02)00239-X.
[109] D.I. Mendoza-Castillo, J.C. Tapia-Picazo, G. Manso-Tápanes, L. Palomino-Asencio, E. García-Hernández, A. Bonilla-Petriciolet, Surface properties of activated carbon fibers obtained from polyacrylonitrile and methyl acrylate: experimental and simulation studies for lead and acid blue 25 dye adsorption from water, J. Mol. Liq. 410 (2024), https://doi.org/10.1016/j.molliq.2024.125621.
[110] N. El Messaoudi, A. El Mouden, M. El Khomri, A. Bouich, Y. Fernine, Z. Ciğeroğlu, J.H.P. Américo-Pinheiro, N. Labjar, A. Jada, M. Sillanpää, A. Lacherai, Experimental study and theoretical statistical modeling of acid blue 25 remediation using activated carbon from Citrus sinensis leaf, Fluid Phase Equilib. 563 (2022), https://doi.org/10.1016/j.fluid.2022.113585.
[111] I.O. Saheed, N.I. Zairuddin, S.A. Nizar, M.A.K.M. Hanafiah, A.F.A. Latip, F.B. M. Suah, Adsorption potential of CuO-embedded chitosan bead for the removal of acid blue 25 dye, Ain Shams Eng. J. (2024) 103125, https://doi.org/10.1016/j.asej.2024.103125.